HHS Public Access

Author manuscript

Acta Biomater. Author manuscript; available in PMC 2021 May 01.

Published in final edited form as:

Acta Biomater. 2020 May ; 108: 111–127. doi:10.1016/j.actbio.2020.03.007.

An Engineered Three-Dimensional Stem Cell Niche in the Inner Ear by Applying a Nanofibrillar Cellulose Hydrogel with a Sustained-Release Neurotrophic Factor Delivery System

Hsiang-Tsun Chang[a], **Rachel A. Heuer**[a], **Andrew M. Oleksijew**[a], **Kyle S. Coots**[a], **Christian B. Roque**[a], **Kevin T. Nella**[a], **Tammy L. McGuire**[b], **Akihiro J. Matsuoka**[a,c,d]

[a]Department of Otolaryngology and Head and Neck Surgery, Feinberg School of Medicine, Northwestern University, Chicago, IL 60611, USA

[b]Department of Neurology, Feinberg School of Medicine, Northwestern University, Chicago IL 60611, USA

[c]Department of Communication Sciences and Disorders, Northwestern University, Evanston, IL 60201, USA

[d]Hugh Knowles Center for Hearing Research, Northwestern University, Evanston, IL 60201, USA

Abstract

Although the application of human embryonic stem cells (hESCs) in stem cell–replacement therapy remains promising, its potential is hindered by a low cell survival rate in post-transplantation within the inner ear. Here, we aim to enhance the *in vitro* and *in vivo* survival rate and neuronal differentiation of otic neuronal progenitors (ONPs) by generating an artificial stem cell niche consisting of three-dimensional (3D) hESC-derived ONP spheroids with a nanofibrillar cellulose hydrogel and a sustained-release brain-derivative neurotrophic factor delivery system. Our results demonstrated that the transplanted hESC-derived ONP spheroids survived and neuronally differentiated into otic neuronal lineages *in vitro* and *in vivo* and also extended neurites toward the bony wall of the cochlea 90 days after the transplantation without the use of immunosuppressant medication. Our data *in vitro* and *in vivo* presented here provide sufficient evidence that we have established a robust, reproducible protocol for *in vivo* transplantation of hESC-derived ONPs to the inner ear. Using our protocol to create an artificial stem cell niche in the inner ear, it is now possible to work on integrating transplanted hESC-derived ONPs further and also to work toward achieving functional auditory neurons generated from hESCs. Our

Corresponding author: Akihiro J. Matsuoka, M.D., D.M.Sc., Ph.D. FACS, 676 N. St. Clair Street Suite 1325 Chicago, IL 60611 U.S.A., Phone: 312-695-4995, Fax: 312-695-3194, amatsuok@nm.org.

7. Author disclosure statement

No authors have commercial associations that might create conflicts of interest with this work.

Declaration of interests

The authors declare that they have no known competing financial interests or personal relationships that could have appeared to influence the work reported in this paper.

findings suggest that the provision of an artificial stem cell niche can be a future approach to stem cell–replacement therapy for inner-ear regeneration.

Graphical abstract

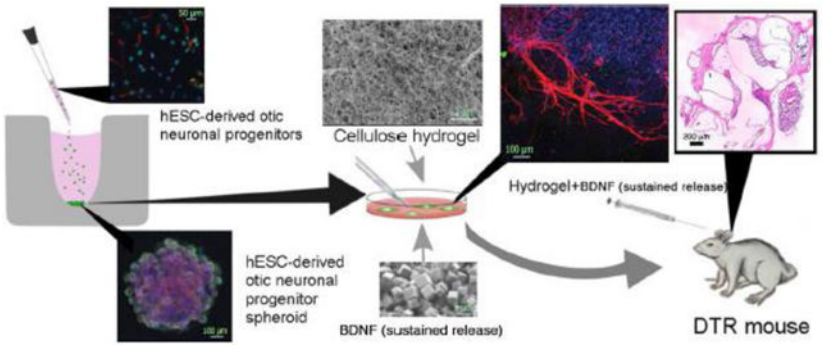

Keywords

Human embryonic stem cells; stem cell niche; spiral ganglion neurons; the inner ear; stem cell–replacement therapy; hydrogel; human pluripotent stem cells

1. Introduction

Between 25 and 48 million United States (US) residents are afflicted with sensorineural hearing loss (SNHL), usually an irreversible condition [1,2]. SNHL typically results from hair cell (HC) loss, initiating a cascade of trans-synaptic degeneration and the secondary loss of obligatory links to the brain, spiral ganglion neurons (SGNs). The degeneration of SGNs follows a distal-to-central progression, peripheral processes degenerating first [3–5]. This pattern has negative implications for successful hearing restoration through cochlear implants (CIs), the only currently available treatment of SNHL [6,7]. Indeed, improvements in CIs' have plateaued in recent years [8,9] due partly to candidates' ears typically having widespread loss of the peripheral processes of SGNs [3,10,11], creating "electrode-neuron gaps" that reduce spatial selectivity. This issue cannot be addressed without correcting this loss.

Stem cell–replacement therapy with human embryonic stem cells (hESCs) has been proposed for restoring damaged HCs and SGNs [12,13]. However, HC replacement is technically challenging, as precise placement in the difficult-to-access scala media is rquired, the diameter of which is less than 1 mm in humans [14]. Furthermore, HC replacement therapy would still require the restoration of SGN peripheral processes and synaptogenesis. Unfortunately, the most promising report to date of stem cell–based therapy showed neither broad nor cochlear-specific restoration of HC-SGN synapses, nor has this report been successfully replicated [15,16].

Our long-term goal, then, is realizing a next-generation "biohybrid" CI that integrates the proven CI approach with human embryonic stem cell–replacement therapy. Such hybrid devices are more practical than stem cell–only approaches, as the latter must overcome the

additional challenge of restoring HCs, as mentioned above. Newly regenerated, stem cell–derived SGN neurites can extend between Rosenthal's canal and the scala tympani [4,14,17–19]. By focusing on human stem cell transplantation to the scala tympani, newly regenerated SGNs can bridge electrode-neuron gaps to improve spatial selectivity, preserve tonotopy, and motivate higher CI-electrode densities, which should increase CI performance, user satisfaction, and overall quality of life. It will also broaden the pool of candidates, thus serving a wider patient population [20].

Stem cells normally reside in microenvironments ("niches") that interact with surrounding cells to regulate and promote proliferation, differentiation, and survival [21,22]. While many questions remain as to which stem cell niche components are fundamental for hESCs to adequately, efficiently differentiate to SGNs, the key players of a stem cell niche generally include cellular components, an extracellular matrix (ECM), and secreted factors [23,24]. In the case of the inner ear, which consists of three primarily fluid-filled chambers—the scala tympani, scala media, and scala vestibuli—all three constituents of a stem cell niche are absent, creating an inhospitable environment for transplanted hESC-derived ONPs [25]. Indeed, previous efforts have been made to transplant hESC-derived ONPs or murine mesenchymal stem cell–derived ONPs into these chambers or even directly into the modiolus where SGNs are housed [26–29]. The survival rate of transplanted cells, however, has been marginally low—on the order of 0.1–1.0% [26,28,30–32]. Therefore, the successful use of stem cell therapy in the inner ear may require the creation of a supportive artificial stem cell niche within the inner ear, though the precise constituents of the normal microenvironment in the inner ear are still unknown.

When transplanted cells are injected into the scala tympani in a dissociated form, the cells first float in the perilymph within the scala tympani and then individually adhere to a layer of squamous epithelium that covers the scala tympani circumferentially [33]. The lack of direct cell contact with other transplanted stem cells, however, can result in insufficient *bona fide* cell-cell adhesion, molecule secretion, and receptor interaction with membrane-bound ligands, leading to poor engraftment and inefficient neuronal differentiation [24]. To circumvent the lack of direct contact in transplanted hESC-derived ONPs in the inner ear, we have generated hESC-derived ONP spheroids [24,34]. We define a "spheroid" as a self-organizing multicellular structure of stem cells consisting of organ-specific progenitors that allow transplanted cells to maintain direct cell contact among each other, thereby maintaining the secretion of cell-cell adhesion molecules and receptors [35]. We hypothesize that this spheroid structure promotes the survival of cells and facilitates otic neuronal differentiation.

The implantation of a hydrogel ECM can also provide a supportive stem cell niche by integrating a mechanical scaffold with the scala's squamous epithelium [36–38]. ECMs can hold transplanted stem cells in place and localize cell-to-cell signaling. Their integration with spheroids can reduce undesirable agglomeration in addition to insulating cells from injection shearing forces that may lead to apoptosis [39].

Nanofibrillar cellulose (NFC) hydrogel, can mimic native soft tissue ECMs in fiber size and mechanical properties [40–42]. An NFC hydrogel is also injectable and thus capable of

delivering cells (such as hESC-derived spheroids) to the desired target. Cellulose is biocompatible, showing moderate foreign body responses, if any, and is safe for stem cell applications, having no known toxicity to hESCs [42–44]. Therefore, we hypothesize that utilizing an NFC hydrogel ECM provides a supportive stem cell niche in the inner ear for hESC-derived ONP spheroids.

Conventional growth factors suffer from fragility and thermo-instability under normal physiological conditions both *in vitro* and *in vivo*, exhibiting short half-lives typically ranging from minutes to hours [45]. So far, this drawback has been addressed by large overprovisions of the requisite growth factor(s) and, in *in vitro* cultures, by frequent media changes to maintain a reservoir of bioactive protein in the culture medium. The polyhedrin delivery system (PODS®) is a crystalline growth factor formulation developed to overcome the limitations of standard soluble growth factors. The PODS® technology has adapted viral machinery to encase a chosen growth factor (i.e., BDNF) into polyhedrin protein cases [46–48]. The resultant growth factor co-crystals have slow degradation profiles under physiological conditions and therefore allow the sustained release of embedded bioactive growth factor protein. We focus on brain-derived neurotrophic factor (BDNF), which promotes survival and neuronal differentiation of SGNs *in vivo* and *in vitro* [49–51]. Degradation of the PODS® crystals is facilitated by cell- and protease-mediated processes, allowing the release of physiologically relevant levels of cargo protein (in this case, BDNF) over several weeks. We hypothesize that PODS®-human BDNF (hBDNF) system stably provides BDNF to hESC-derived ONPs, facilitates otic neuronal differentiation, and improves the engraftment of transplanted cells.

The purpose of this study is to create an artificial stem cell niche using hESC-derived ONP spheroids, NFC hydrogel, and a self-sustaining source of BDNF to promote the survival and neuronal differentiation of transplanted hESC-derived ONPs. In this study, we first examined the effects of the NFC hydrogel and PODS®-hBDNF on hESC-derived ONP spheroids *in vitro*, followed by *in vivo* analysis using diphtheria toxin (DT) receptor–positive mice (DTR mice) [52–54]. In the DTR mouse model, the gene for human DT receptor (hDTR) was inserted under the regulation of the promoter for *Pou4f3*, an HC-specific transcription factor [52]. The DTR mouse model serves as a suitable model for our long-term aim (i.e., designing a “biohybrid” CI) because a single DT injection at postnatal day 28 (P28) results in HC wipeout with retention of SGNs [55]. This feature provides us with hESC-derived ONP spheroids to bridge the electrode-neuron gaps between extant SGNs and future biohybrid CI electrodes. We also used a DTR mouse model for this study to create HC damage rather than SGN damage in the bony modiolus because surgical access to the bony modiolus poses significant risks of cerebrospinal fluid leaks and of damaging modiolar blood vessels [14,33], complications that can result in meningitis and inner-ear ischemic stroke.

Toward these ends, we characterized the survival and neuronal differentiation of the embedded hESC-derived ONPs in an artificial stem cell niche using immunocytochemistry and immunohistochemistry along with the viscoelastic and rheological analysis of the NFC hydrogel. Our findings suggest that this combination of factors may enable a future approach to stem cell–replacement therapy for inner-ear regeneration.

2. Materials and methods

2.1. Differentiation of human embryonic stem cells into otic neuronal progenitors

The hESC lines H1, H7, and H9 were used in this study (WiCell, Madison, WI, USA). ONPs were generated based on our previously established protocol [56]. See also the Supplemental Data in detail. A stepwise series of ligands and growth factors was added to a neuronal induction medium (NIM) to promote hESC differentiation toward a late-stage ONP lineage (Fig. 1).

2.2. Three-dimensional spheroid culture with nanofibrillar cellulose hydrogel

The hESC-derived late-stage ONPs were seeded into a 96-well Clear Round Bottom Ultra-Low Attachment Microplate® (#7007; Corning Life Science, Tewksbury, MA, USA) at 50,000 cells per well and centrifuged at 900 rpm for 20 minutes followed by incubation at 37˚C for two days. Late-stage ONP spheroids were also generated by seeding 1 million cells into an EZSPHERE® culture plate (#2641701; Nacalai USA, CA, USA) at 37˚C for two days. A 96-well Flat-Bottom Clear Plate® (Greiner Bio-One, Nürtingen, Germany) was loaded with GrowDex®-T (#200103010; UPM-Kymmene Corporation, Helsinki, Finland) pre-mixed with 800,000 PODS®-hBDNF (#PPH1–50; Cell Guidance Systems, Cambridge, UK) or 20 ng/mL of recombinant human BDNF (RhBDNF) (R&D System, Minneapolis, MN, USA). Spheroids were then carefully transferred from culture plates to a flat-bottom plate with direct injection into the GrowDex®-T solution. GrowDex®-T was diluted to 0.5% (w/v) and 0.375% (w/v) throughout the *in vitro* study based on the manufacturer's instructions. Anionic NFC hydrogel (GrowDex®-T) was kindly provided by the UPM-Kymmene Corporation (Helsinki, Finland). Cellulose kraft pulp was chemically modified and fibrillated to form anionic NFC hydrogels, the diameter of which ranged from 4–10 nm and lengths from 500–10,000 nm, which were measured using electron microscopy. PODS®-hBDNF was kindly provided by Cell Guidance System (Cambridge, UK). NeuroFluor™ NeuO (#01801; STEMCELL Technologies, British Colombia, Canada) was used for the detection of live neurons.

2.3. Immunocytochemistry (monolayer culture)

Immunocytochemistry on cells cultured on a two-dimensional (2D) monolayer was performed based as previously described [56]. See also the Supplemental Data for further details. The primary and secondary antibodies used in this study are also listed in Supplementary Tables S1 and S2, respectively. Immunocytochemistry controls were also performed as previously described [57,58]. The primary antibody controls were performed with immunocytochemistry with the primary antibody and hESC-derived ONPs with a second primary antibody to each antigen [57]. Secondary antibody controls were performed each time multiple primary antibodies were used [57]. Labeling controls (detection controls) were performed for a sample from each batch of hESC culture [57]. See Supplementary Fig. S1 for exemplary figures for these control conditions.

2.4. Immunocytochemistry (three-dimensional spheroid culture)

For hESC-derived late-stage ONP spheroids, culture medium was first removed and spheroids were fixed with 4% (w/v) paraformaldehyde for 30 minutes followed by blocking overnight in a solution composed of 5% bovine serum albumin (Sigma-Aldrich, St. Louis, MO, USA) and 0.1% Triton X-100 in Dulbecco's Phosphate-Buffered Saline (Corning Life Sciences, Tewksbury, MA, USA). Each sample was incubated for three days at room temperature with the primary antibodies listed in Supplementary Table S3. This was followed by several phosphate-buffered saline (PBS) washes and incubation in the dark for three days at room temperature with Alexa Fluor 488 and 647 (#ab150129, #ab150075; Abcam, Cambridge, MA, USA). Nuclei were stained with 4' 6-diamidino-2-phenylindole (DAPI; #D1306; Thermo Fisher Scientific, Waltham, MA, USA) for 30 minutes. Images were then assessed using a Nikon A1 confocal microscope (Nikon, Tokyo, Japan). ImageJ ver. 2.0.0-rc-69/1.52p. (National Institutes of Health, Bethesda, MA, USA) was used to quantify the images. Further details on image acquisition and quantification of immuno-positive cells are described in the Supplementary Data.

2.5. Enzyme-linked immunosorbent assay for brain-derived neurotrophic factor

To measure the concentration of BDNF secreted from PODS® crystals, the culture media from both a control and an experimental condition were collected at each time point and immediately stored at −80˚C before running an enzyme-linked immunosorbent assay (ELISA). The same method was applied to measure the degradation of RhBDNF. All samples were quantified with a BDNF ELISA kit (#BGK23560; PeproTech, Rocky Hill, NJ, USA), and the results were analyzed with a Synergy HTX Multi-Mode Reader (BioTek, Winocski, VT, USA) at a 450-nm wavelength, as instructed by the manufacturer.

2.6. Rheological characterization of nanofibrillar cellulose hydrogel

Rheological characterization was performed on an MCR302 Rheometer (Anton Paar, Graz, Austria) using a 25-mm diameter plate at 37˚C. Each sample was dispensed on the preheated rheometer plate with a gap distance of 1 mm, and excess hydrogel was removed. The testing protocol was then applied to the sample. Each hydrogel sample was used for only one test.

2.7. Quantitative real-time polymerase chain reaction (RT-qPCR)

RNA extraction and quantitative real-time reverse transcriptase polymerase chain reaction (RT-qPCR) were performed using standard techniques. Further details of the method and primers used for RT-qPCR can be found in the Supplementary Data.

2.8. Deafening and genotyping of diphtheria toxin receptor–positive mice

The Institutional Animal Care and Use Committee (IACUC) of the Northwestern University Feinberg School of Medicine approved our experimental procedures (IACUC Protocol number: IS00011516). The protocol was also reviewed and approved by the US Army Animal Care and Use Review Office. Both male (N=18) and female (N=19) DTR mice (3–6 months old) were used as hESC-derived ONP recipients. Ten wild-type (WT) C57/BL6 mice were used as a control. We chose a deaf-animal model in the DTR mouse group and developed a colony from a contribution of DTR mice provided by Dr. W. Edwin Rubel

(University of Washington, Seattle, WA, USA). The DTR mice were deafened at a young-mature age (P28–P35) using a single intramuscular injection of DT at a dose of 25 ng/g (intramuscular injection), causing HC degeneration [53,54,59]. For identification of DTR mice (*Pou4f3*$^{DTR/+}$) and WT mice (*Pou4f3*$^{+/+}$), a tail biopsy was collected and DNA was extracted using a DNA blood and tissue kit (Qiagen, Germantown, MD, USA). The target allele was amplified using a Mastercycler® nexus (Eppendorf, Hamburg, Germany) and the primer (0.4 μM) listed in the Supplemental Data. For further details, see the detailed description of PCR in the Supplementary Data.

2.9. Auditory brain stem response

Hearing loss induced by DT injection was confirmed by auditory brain stem response (ABR) recordings before and after injection. DTR mice were anesthetized with 67 mg/kg of ketamine and 3.3 mg/kg of xylazine (intraperitoneal injection with additional dosing of ketamine as needed). Both tone-burst and click-evoked ABRs were used to assess the sensitivity of the nerve to acoustic stimuli to confirm the efficacy of the DTR mouse model. Both stimulus control and averaging were performed using TestPoint (Cape Town, South Africa) as well as SmartEP (Intelligent Hearing Systems, Miami, FL, USA). A detailed description of the ABR parameters and settings is provided in the Supplementary Data. We performed tone burst–evoked ABR on both three DTR mice and four WT mice to thoroughly test the frequency-specific hearing threshold. Click-evoked ABR was performed on the remaining mice.

2.10. Transplantation of human embryonic stem cell–derived otic neuronal progenitors

Human ESC-derived ONPs were transplanted in left cochleae. Right cochleae were used as a control condition. Meloxicam (2 mg/kg, subcutaneous injection) was given prior to surgery to minimize respiratory distress; follow-up doses (1 mg/kg/day) were given for three days. Anesthesia was induced with isoflurane at 3–4% (reduced to 1–2% after induction) and was delivered with oxygen (0.3 L/min) and nitrous oxide (0.25 L/min) gas. The animals' heads were secured to a custom head-holder that delivered the anesthetic gas. Body temperature was maintained by a circulating water pad, and insensate fluid loss was replaced at 0.1 mL/10g (body weight). A post-auricular incision was made, and bone (caudal to the stylomastoid foramen) was removed with a surgical drill to reveal the round window. The round window membrane was then excised using a 30–33 G needle. Dissociated hESC-derived ONPs (250,000 cells) or hESC-derived ONP spheroids (five spheroids, each containing 50,000 ONPs) were delivered to the scala tympani by a glass micropipette while manipulating the pipette's pressure with a Xenoworks Digital Injector (Sutter Instrument, Navato, CA, USA). The pressure range used for a spheroid transplantation was between −1 hPa and +5 hPa. Two μL of 1% GrowDex®-T with 800,000 of PODS®-hBDNF were delivered using a 10-μL Hamilton syringe. After the transplantation was completed, the round window was covered by a small piece of fascia and secured with Vet Bond™ adhesive (3M, Minneapolis, MN, USA). Muscle and skin were closed in layers, and the animal was allowed to recover with thermal therapy. The animal was kept for 90 days, allowing engraftment and neuronal differentiation in the inner ear. No immunosuppressant was administered postoperatively [26,30].

2.11. Immunohistochemistry

After completion of the post-implantation survival period, each animal was euthanized, the cochlea was dissected, and the specimen was sectioned into 10-μm slices on a Leica CM3050 S cryostat (Leica Inc., Nussloch, Germany). Immunohistochemistry was performed using standard techniques with a mouse anti-human nuclear antibody (AHNA) (1:100, STEM101, Takara Bio, Tokyo, Japan) and a rabbit anti-β-III tubulin antibody (1:500, Abcam, Cambridge, MA, USA). See further details on this process in the Supplementary Data. Both positive and negative control conditions were obtained to ascertain the specificities of AHNA (Supplementary Fig. S2). Laser scanning confocal imagery was performed with a Leica TCS SP5 microscope (Leica Inc., Nussloch, Germany). Whole-mount HC staining was also performed on a WT mice, as well as DT-injected DTR mice, and non-DT-injected DTR mice. Further details can be found in the Supplementary Data.

2.12. Neurite-bearing, neurite growth, and neurite arborization assays

The pan-neuronal marker β-III tubulin was used to visualize neurite-bearing cells, measure neurite length, and calculate neurite arborization area. The analysis was performed by examining an individual confocal optical Z-stack section through the entire extent of each spheroid at the observation time point using ImageJ ver. 2.0.0-rc-69/1.52p (National Institute of Health, Bethesda, MD, USA) [60]. Further details can be found in the Supplementary Data.

2.13. Quantification of the surviving anti-human nuclear antibody-positive cells in the inner ear

The total profile number was calculated by the counting profiles of the $AHNA^+$ cells [61,62]. Only cells with the confirmation of AHNA-positive immunostaining were counted as surviving ONPs. The total profile number of the AHNA-positive cells was determined for each of the five sections of each animal in four anatomic subdivisions of the cochlea: basal turn, mid-turn, apical turn, and modiolus [63]. A more detailed description of the quantification, including Abercrombie's method of estimating the number of cells from profile counts, can be found in the Supplementary Data [61].

2.14. Calcofluor white staining for nanofibrillar cellulose hydrogels

The presence of NFC in a transplanted cochlea was evaluated with Calcofluor White staining (Sigma-Aldrich, St. Louis, MO, USA). Calcofluor white is a non-specific fluorochrome that binds to cellulose and chitin in cell walls [64]. Three DTR mice transplanted with GrowDex-T and PODS® were used. Due to fluorescence crossover between Calcofluor White and DAPI, no counterstain was used. Further details can be found in the Supplementary Data.

2.15. Hematoxylin and eosin (H&E) histology

Hematoxylin and eosin (H&E) staining was performed on transplanted DTR mouse cochleae to examine the extent of tissue response from xenograft transplantation. Further details of the H&E staining method can be found in the Supplementary Data.

2.16. Detection of major histocompatibility complex class I and class II antigens by flow cytometry

Flow cytometry assays were performed on both hESCs (H9), hESC-derived ONP spheroids, and human embryonic kidney cells (HEK 293 cells: control) using a BD LSRFortessa™ (BD Biosciences, San Jose, CA, USA) using standard protocol. Major histocompatibility complex (MHC) class I and class II antigens were used as transporters because they play critical roles in immune rejection in xenograft [65]. Further details of this method are outlined in the Supplementary Data.

2.17. Statistical analysis

When appropriate, and as indicated in each figure, statistical analysis was performed. Three biological and technical replicates were obtained and used for statistical analysis unless otherwise noted [66,67]. Experimental values are typically expressed as means ± standard error. All statistical analyses were performed with R (version 3.5.1. 2018-07-02, Vienna, Austria) [68]. Normal distributions were assumed. An analysis of variance (one-way) with Bonferroni-corrected *post hoc* t-tests or two-tailed t-tests was performed. P values smaller than 0.05 were considered statistically significant.

3. Results

3.1 Neuronal differentiation of human embryonic stem cell–derived otic neuronal progenitors with the polyhedrin delivery system

The human ESCs H1, H7, and H9 were sequentially differentiated into late-stage ONPs using the protocol outlined in Fig. 1 and then treated with 800,000 of PODS®-hBDNF for seven days in NIM or BrainPhys™ (Fig. 2A). Compared to late-stage ONPs (Fig. 2B), the treated cells presented more bipolar-shaped neurites, which is consistent with the morphology of human SGNs (Fig. 2C) [69]. After seven days of treatment, late-stage ONPs highly expressed GATA3 (an otic lineage marker) [70,71], Neurogenin-1 (NeuroG1, an otic lineage marker) [72,73], PAX8 (an otic lineage marker; more specifically marking the otic placode and otic vesicle) [74,75], SOX2 (a neuronal progenitor marker) [70], nestin (a neuronal progenitor marker) [70], vesicular glutamate transporter-2 (VGLUT2, a glutamatergic neuronal marker) [76], β-III tubulin (a pan-neuronal marker) [77,78], and peripherin (a peripheral sensory neuron marker) [79] (Fig. 2D–I). PODS®-hBDNF-treated ONPs did not express E-cadherin (ECAD, an otic epithelial marker) [80], PAX6 (a central nervous system neuronal marker) [81], nor SOX10 (a glial marker) [82] (data not shown), suggesting that the cells differentiated toward otic neuronal lineage instead of an otic-epithelial lineages, central nervous system neuronal lineages, or glial lineages.

With PODS®-hBDNF treatment of the late-stage ONPs, the proportion of nestin and SOX2 positive cells were expressed significantly less than other markers, suggesting that the treatment facilitated otic neuronal differentiation (Fig. 2J). In the quantification of PAX8, nestin and SOX2-positive cells, the PODS® treatment significantly decreased the positivity of nestin (from 71.3% ± 3.42 to 41.0% ± 4.35) and that of SOX2 (from 64.2% ± 2.35 to 45.2% ± 2.90) compared to RhBDNF treatment, suggesting that PODS® treatment more effectively differentiated the late-stage ONPs into otic neuronal lineages (Fig. 2K). However,

there were no statistically significant differences in the expression of PAX8 between RhBDNF (99.6% ± 0.294) and PODS®-hBDNF treatment (99.8% ± 0.222) (Fig. 2K).

3.2. The generation of human embryonic stem cell–derived otic neuronal progenitor spheroids

The hESC-derived ONP spheroids were generated from dissociated late-stage ONPs using an EZSPHERE® or 96-well Clear Round Bottom Ultra-Low Attachment Microplate® (Fig. 3A–B). A live neuron assay was performed to evaluate the viability of an hESC-derived ONP spheroid cultured in NIM/Brainphys™ after seven days. An hESC-derived ONP spheroid was labeled with 0.25 μM of NeuroFluor™ NeuO and incubated for one hour (shown in green in Fig. 3C), demonstrating that the spheroid was β-III tubulin–positive [83]. The control condition can be found in Supplementary Fig. S3. A 3D immunocytochemical analysis also indicated that hESC-derived ONP spheroids expressed the positivity of PAX8, β-III tubulin, and nestin when cultured in NIM/BrainPhys™ for seven days (Fig. 3D), suggesting that the spheroids were differentiating into otic neuronal lineages.

3.3. Rheological and viscoelastic properties of nanofibrillar cellulose hydrogel

Before performing a 3D culture of hESC-derived ONP spheroids with NFC hydrogel, the mechanical properties of the hydrogel were first rheologically characterized by frequency sweep testing (Fig. 4A). The frequency sweep in Fig. 4A shows the previously reported characteristic behavior of NFC hydrogel: The loss factor (tan δ=G”/G’) was much lower than 1 [40]. This finding demonstrates its gel-like structure. This behavior is also nearly independent of the frequency. In addition, 0.375% GrowDex®-T showed a higher loss factor (tanδ=G”/G’) than both 0.5% and 1% GrowDex®-T. Viscosity over shear stress was also measured to optimize the concentration suitable for the injection of GrowDex®-T, and 1% GrowDex®-T showed higher viscosity than both 0.5% and 0.375% GrowDex®-T at lower shear stresses (Fig. 4B). At high stress levels (> 20 Pa, applicable to injections), it also exhibited more fluid-like behavior (Fig. 4B). Shear moduli (G) of different concentrations of GrowDex®-T were estimated to determine their rigidities. In Fig. 4C, 1% GrowDex®-T demonstrates a disproportionally higher shear modulus than both 0.5% and 0.375% GrowDex®-T above a 7% shear strain.

3.4. In vitro culture of human embryonic stem cell–derived otic neuronal progenitor spheroids with nanofibrillar cellulose hydrogel

After the rheological characterization, we cultured hESC-derived ONP spheroids with 0.375% GrowDex®-T for seven days. Fig. 4D shows a schematic diagram of this part of the experiment. Three-dimensional immunocytochemistry was then performed to assess the positivity of PAX8, β-III tubulin, MAP2 (a neuronal cytoskeleton marker) [84,85], VGLUT2, and peripherin to show that hESC-derived ONP spheroids were expressing otic neuronal signals (Fig. 4E–G).

3.5. Quantitative real-time polymerase chain reaction on human embryonic stem cell–derived otic neuronal progenitor spheroids with nanofibrillar cellulose hydrogel

Fig. 4H demonstrates that qRT-PCR on hESC-derived ONPs spheroids cultured in 0.375% GrowDex®-T and 800 K of PODS®-hBDNF for seven days showed more down-regulation of PAX8 and up-regulation of MAP2, VGLUT2, peripherin, and β-III-tubulin than hESC-derived ONPs spheroids cultured in Brainphys with 20 ng/mL RhBDNF for seven days.

3.6. Enzyme-linked immunosorbent assay for brain-derived neurotrophic factor

Before the use of PODS®-hBDNF with our ONP spheroi culture, we quantified the release kinetics of PODS®-hBDNF using ELISA. The concentration we detected from the supernatant of NIM containing 800,000 of PODS®-hBDNF showed steady zero-order release kinetics of hBDNF from PODS®-hBDNF with approximately 25–50 pg/mL per day (Fig. 5A–B). Although PODS®-hBDNF crystals were encased in different concentrations of GrowDex®-T (i.e., 0.5% vs. 0.375%), both groups showed similar release profiles with a total amount of approximately 300 pg/mL over seven days (Fig. 5A–B). On the contrary, a one-time dosage of 20 ng/mL of RhBDNF provided a sufficient amount of hBDNF on the first day, but after three days, the active hBDNF left in both the culture media had less than 100 pg/mL (Supplementary Fig. S4). Finally, we evaluated endogenously secreted hBDNF from hESC-derived ONP spheroids. An ONP spheroid (with cell density of 50,000 cells/spheroid) was cultured in NIM without PODS®-hBDNF. There was virtually no BDNF detected in this NIM-only condition with the ELISA spheroids (shown in green in Fig. 5A–B).

3.7. In vitro culture of human embryonic stem cell–derived otic neuronal progenitor spheroids with nanofibrillar cellulose hydrogel and a polyhedrin delivery system

The hESC-derived ONP spheroids were further cultured with GrowDex®-T and PODS®-hBDNF for seven days. The schematic diagram in Fig. 6A shows this part of our experiment. Phase-contrasted images of hESC-derived ONP spheroids cultured in GrowDex®-T and PODS®-hBDNF demonstrate that the integrity of the spheroids tended to decline more with GrowDex®-T and PODS®-hBDNF than with only GrowDex®-T over 48–72 hours (Fig. 6B(a–c) vs. Fig. 6B(e–f)). The image also shows that the cells in the spheroids may have been migrating toward PODS®-hBDNF crystals, suggesting that a BDNF gradient may be attracting hESC-derived ONPs in a chemotactic fashion (Fig. 6B(f), white arrow). Fig. 6C–F and Fig.7 A–D show the immunocytochemistry of hESC-derived ONP spheroids cultured with 0.5% and 0.375% GrowDex®-T, respectively, for seven days. As seen in Fig. 6B, hESC-derived ONP spheroids maintained the integrity of their spheroidal shapes better when they were cultured without GrowDex®-T or PODS®-hBDNF (Fig. 6C).

The quantification of PAX8 expression in immunocytochemistry demonstrates the advantages of GrowDex®-T and PODS®-hBDNF in enabling otic neuronal differentiation. We chose PAX8 expression to gauge the degree of otic neuronal differentiation, as PAX8 expression is known to peak at the otic placode or otocyst stages (corresponding to the ONP stage) [86,87] and then to down-regulate afterward [86–88]. Fig. 7E demonstrates that PAX8-positive cells are significantly more common in NIM-only conditions (97.7% ± 0.14 for 0.5% GrowDex®-T and PODS®-hBDNF and 99.0% ± 0.44 for 0.375% GrowDex®-T

and PODS®-hBDNF; shown in green bars) compared to other conditions. This finding suggests that GrowDex®-T in conjunction with PODS®-hBDNF can facilitate otic neuronal differentiation. This finding is also apparent in the second rows of Fig. 6C–F and Fig. 7A–D, which show that the positivity of PAX 8 was most obvious under NIM-only conditions.

The quantification of neurite lengths in hESC-derived ONP spheroids demonstrates significantly longer neurites in the spheroids that were cultured in the combination of GrowDex®-T and PODS®-hBDNF (Fig. 7F). The number of neurite-bearing cells in the ONP spheroids was significantly smaller when they were cultured under NIM-only conditions (Fig. 7G). Finally, a similar trend was observed in our neurite arborization assay as in the neurite growth assay (Fig. 7F) in that axonal branching was significantly greater in a culture condition with both GrowDex®-T and PODS®-hBDNF (Fig. 7H).

3.8. In vivo transplantation of human embryonic stem cell–derived otic neuronal progenitor spheroids into the inner ear

Fig. 8A shows the experimental paradigm of this part of the study. Prior to stem cell transplantation in the inner ear, both tone burst–evoked and click-evoked ABRs were used to assess the sensitivity of the inner ear to acoustic stimuli to confirm the efficacy of the DTR mouse model. Fig. 8B and 8C shows exemplary data of typical tone burst–evoked ABR waveforms on a WT C57/BL6 mouse (Fig. 8B) and a deafened DTR mouse (Fig. 8C). A level- and frequency-series of tone burst–evoked ABRs demonstrated that a DTR mouse had no detectable ABRs even at the lowest attenuation levels (i.e., 0 to −20 dB, equivalent to 100 to 120 dB SPL) (Fig. 8C). Fig. 8D shows exemplary data of click-evoked ABR waveforms for a WT mouse (left column) and a deafened DTR mouse (right column). The deafened DTR mouse demonstrated no detectable waves I or V even with the highest stimulation levels, indicating that it was adequately deafened for the study. Fig. 8E shows the plots of ABR threshold audiograms of three DTR mice injected with DT and of eight WT mice. For each DTR mouse, no ABRs were detected at any tested frequency. Fig. 9A shows immunohistochemistry of the cochleae of WT mice and DTR mice. Confocal fluorescence images of phalloidin (red) and myosin VIIa (green) in the whole-mounted auditory epithelium demonstrate intact HCs in both a WT and a DTR mouse without DT injection (control conditions are shown in Fig. 9A(a) and (b)). On the contrary, a P28 DT-treated mouse DTR with DT injection shows no signs of inner or outer HCs demonstrating ablation by DT throughout the cochlea (Fig. 9A(c) shows the basal turn and (d) the apical turn).

The hESC-derived ONP spheroids were then transplanted into the DTR mice cochleae. After 90 days, hESC-derived ONP spheroids transplanted into the inner ear with 1% GrowDex®-T and PODS®-hBDNF were engrafted in the scala vestibuli (Fig. 9B(a)) and in the scala tympani (Fig. 9B(b–c)). As Fig. 9B shows, the transplanted cells still maintained aggregated forms in the inner ear. Fig. 9B(b) also demonstrates that hESC-derived spheroids lodged in the wall of the scala tympani and extended neurites toward the modiolus (white arrow). A dissociated form of stem cell transplantation can be found in Supplementary Fig. S5.

We then performed quantification of the engrafted hESC-ONP spheroids. The AHNA+ profiles indicate that the engrafted ONP spheroids tended to lodge more in the basal turn of the cochlea than the mid- or apical turns (Fig. 9C(a)). Also, hESC-derived ONPs with

dissociated forms did not survive as efficiently as those with spheroid forms (Fig. 9C(b)). Engraftment was significantly better with GrowDex®-T and GrowDex®-T with PODS®-hBDNF (Fig. 9C(c)). Further quantitative analysis confirmed that GrowDex®-T with PODS®-hBDNF promoted the neurite extension of engrafted hESC-derived ONPs *in vivo* (Fig. 9C(d)). Finally, the overall survival rate of our transplanted spheroids with GrowDex®-T and PODS®-hBDNF after 90 days was approximately 0.1% (see the Supplementary Data for further details). We evaluated the presence of NFC hydrogel in the transplanted cochlea using Calcofluor White staining. Fig. 9D shows that the NFC hydrogel was present for 7 days (Fig. 9D(b)) and also 90 days (Fig. 9D(c)) after transplantation.

Finally, immunorejection was evaluated with H&E staining, as our transplant was xenografted (i.e., human stem cells to mice). Fig. 9E(a) shows a control cochlea without transplantation; that is, there was no areolar fibrous tissue or any lymphocyte infiltration noted. Fig. 9E(b) and (c) show an hESC-transplanted cochlea with GrowDex®-T and PODS®-hBDNF (on day 7 and 90, respectively). In Fig. 9E(b), there is mild areolar fibrous tissue infiltration in the scala vestibuli (red circle). Fig. 9E(c) shows lymphocyte aggregation and dilated blood vessels in the surrounding area of the transplanted cochlea but little overall cell response inside the membranous labyrinth.

Fig. 9F shows protein expression of MHC class I and MHC class II antigen assessed by flow cytometry in undifferentiated H9 hESCs (upper row) and hESC-derived ONP spheroids (lower row). Both undifferentiated H9 hESCs and hESC-derived ONP spheroids demonstrated no detection of MHC class I or MHC class II antigens. Positive-control of flow cytometry can be found in Supplementary Fig. S6.

4. Discussion

The number and integrity of surviving SGNs have been implicated in the hearing sensitivities of deafened patients reliant on CIs or future stem cell–replacement therapy [77,89,90]. A sustained ability to repopulate SGNs would enable improved clinical results [10,91–94]. Moreover, while HC regeneration is an important research area, successful inner-ear function will still depend on the effective transmission of electrical signals to the brainstem via SGNs. Therefore, new techniques to enhance the efficiency of stem cell–derived ONP transplantation to augment extant SGN populations are critical. Historically, the low overall survival of stem cell–derived ONPs transplanted into the inner ear can be attributed to its relatively inhospitable environment and its inadequate levels of trophic factor [26,30,63,95]. To overcome these issues, we created an artificial stem cell niche using hESC-derived ONP spheroids, NFC hydrogel, and a self-sustaining source of BDNF to promote the survival and neuronal differentiation of transplanted hESC-derived ONPs. We used hESCs-derived ONPs to generate spheroids, as their use is more clinically relevant to the core interests of the study than autologous murine stem cells. In addition, human and murine stem cells behave drastically different in culture. For instance, there are profound differences in cell cycle regulation, control of apoptosis, and cytokine expression between the two [96]. Given that the majority of ongoing clinical trials use human pluripotent stem cells, our work represents a significant step in advancing stem cell replacement therapy in the human inner ear.

Immunocytochemistry of our monolayer culture revealed that hESC-derived ONPs cultured with PODS®-hBDNF for seven days expressed adequate markers for human SGNs, a finding consistent with our previously reported data [56,63,70,87]. We also performed qRT-PCR, demonstrating that our hESC-derived ONP spheroids also had otic lineages, although not identical to human SGNs [56]. Notably, hESC-derived ONPs were mostly peripherin-positive, which is more consistent with type II human SGNs [97], although this is consistent with a previous result on mouse ESC–derived ONPs [98].

In addition, PODS®-hBDNF treatment on hESC-derived ONP spheroids showed that it promoted otic neuronal differentiation, as it significantly decreased nestin- and SOX2-positive cells; however, PAX8-positive cells did not significantly differ between RhBDNF treatment and PODS®-hBDNF treatment. Our immunocytochemistry data and qRT-PCR data on hESC-derived ONP spheroids, however, indicated significantly decreased PAX8-positive cells in PODS®-hBDNF and GrowDex®-T, suggesting that our artificial stem cell niche promoted further neuronal differentiation than a 2D-monolayer ONP culture with PODS®-hBDNF [74]. A qRT-PCR confirmed that hESC-derived ONP spheroids were guided toward otic glutamatergic neural lineages (Fig. 4H).

We performed a rheological analysis of NFC hydrogel for two reasons. First, the GrowDex®-T we used in this study was an anionic-charged NFC hydrogel, which is different than GrowDex® (neutrally-charged NFC hydrogel) [40]. The rheological characteristics of NFC hydrogel, including swelling properties, can be affected by the extent to which the hydrogel is ionized. Second, the original concentration of GrowDex®-T was 1%; however, microscopic visualization of the cells in 1% GrowDex®-T was extremely challenging, so we diluted it to 0.5% and 0.375% to determine the cells' rheological characteristics. The growing frequency sweep in the NFC hydrogels demonstrated that all the NFC hydrogel samples had approximately tanδ (G"/G') ~0.08–0.13 (gel-like structures) and little frequency dependence, which is a characteristic of self-standing elastic gels. The influence of shear stress on the viscosity of the 1% and 0.5% NFC hydrogels indicated reversible gelation because fluid-like behavior was observed at high shear stress levels (> 10 Pa for 0.5% and > 20 Pa for 1% NFC hydrogel), whereas gel-like behavior was observed at low shear stress levels. This finding is consistent with previous studies that used NFC hydrogel and other physiological hydrogels [40,42,99,100]. However, the 0.375% NFC hydrogel did not demonstrate this feature, presumably because of its high-water content.

A strain sweep of the NFC hydrogels indicated that both the 0.375% and 0.5% NFC hydrogels showed nearly linear deformation in the entire measured strain regions (1–15%) due to their higher water content. However, the 1% NFC hydrogel deviated from linearity above a 7% shear strain. This disproportionally higher shear modulus shows that the yield stress was not directly proportional to the concentration of the 1% hydrogel above a 7% shear strain. This finding can be attributed to the composition of 1% hydrogel containing more cellulose, which formed fiber-like aggregates at higher shear strains. This "shear thinning" behavior of the 1% hydrogel (which we used) made it an attractive ECM for our clinical application, as it allowed the encasing of hESCs in the gel in a low–shear force environment. NFC hydrogel also allowed smooth injections by syringe (high shear force) into the inner ear.

Our ELISA results showed a steady rate of release of RhBDNF from PODS® crystals at approximately 25–50 pg/mL/day, at which rate both *in vitro* and *in vivo* immunocytochemistry demonstrated more promotion of otic neuronal differentiation and enhanced axonal growth on transplanted ONPs than RhBDNF at 20 ng/mL/day. Our *in vitro* and *in vivo* results support the notion that, with the use of PODS®-hBDNF, BDNF concentrations of 25–50 pg/mL were sufficient for hESC-derived ONPs to differentiate into otic neuronal lineages.

Notably, the endogenous secretion of BDNF from hESC-derived ONPs was not detected by ELISA, either because hESC-derived ONPs did not actually secrete BDNF or the ONPs themselves consumed it. In other words, the release of 25–50 ng/mL/day of BDNF might have been greater because the ELISA measurement did not consider consumed BDNF (i.e., by hESC-derived ONPs). While the exogenous provision of hBDNF with the polyhedrin delivery system promoted otic neuronal differentiation in our study, the degradation kinetics of PODS® crystals by any protease and long-term sequelae after more than 90 days is still undetermined. Further studies will be needed to investigate the endogenous provision of BDNF from hESC-derived ONPs.

Multicellular spheroids consist of viable cell rims and central necroses, which typically arise at spheroid diameters of 400–600 μm [101], a finding determined by fluorescence microscopy. Our hESC-derived ONP spheroids lacked fluorescence signals in their centers (Fig. 6–7), however. There are two possible explanations for this absence: 1) a limitation of the blood supply or removal of the waste product caused by hypoxia [101] or 2) a lack of fluorescent antibody penetration to the core. In the latter case, mixing a low number of PODS®-hBDNF crystals during ONP spheroid generation or reducing the total number of cells in individual spheroids may be methods to reduce the sizes of the central necroses. Further studies using hypoxia assays will be required to shed light on this matter.

Previous studies have shown that hESC-based stem cell therapy in the inner ear is hindered by poor engraftment [26,28,63]. The majority of transplanted, dissociated hESCs were either unable to attach to the lining of fluid-filled inner-ear scalae or, even if they attached, the lack of aggregation initiated apoptosis cascades, resulting in cell death [28,63]. After our *in vivo* hESC-derived ONP transplantation, ONPs were found in various scalae in aggregated formations presumably because of 1) the 3D nature of the transplanted ONP spheroids, 2) the NFC hydrogel facilitating their attachment to the lining of scalae, and 3) the continuous release of BDNF by a polyhedrin delivery system.

Our study demonstrated that hESC-derived ONP spheroids transplanted into artificial stem cell niches survived for 90 days at a noteworthy survival rate of 0.1% without the use of immunosuppressant medication. While it is difficult to compare, most of the previous stem cell transplantation studies in the inner ear demonstrated a similar survival rate with much shorter survival duration (1–4 weeks) [26,28,30–32,102,103]. They also used immunosuppressants. The low immunogenicity of hESCs has at least three possible reasons. First, undifferentiated hESCs express low levels of MHC class I and class II molecules in both undifferentiated and differentiated states [104–106]. For this reason, we performed flow cytometry on our hESC-derived ONPs. Our results were consistent with those of previous

studies (Fig. 9F). Second, hESCs lack co-stimulatory molecules, such as CD 80 and CD 86, which are essential for attacking transplanted hESCs in immunorejection responses [105]. Third, hESCs suppress dendritic cell-mediated T-cell proliferation [107]. Fig. 9E(c), for instance, shows a mild amount of lymphocyte aggregation in the surrounding tissue of the transplanted cochlea. Fourth, the inner ear is an “immune-privileged” organ due to its tight, junction-based blood-labyrinthine barrier, similar to the eyes and the brain [108–110]. Finally, a mesh-size analysis of NFC hydrogels indicated that the average mesh size was ~35 nm [111]. The diameters of macrophages and lymphocytes (critical players in immunorejection) range from 20–30 μm in size, which is approximately 10^3 times greater than the mesh size, so the nano-pore size of NFC hydrogels might have prevented immunorejection by blocking their entry. Further studies in the immune rejection will be required to investigate this issue before a clinical transition.

Human SGNs are bipolar neurons [69]; however, the hESC-derived ONP spheroids extended multipolar neurites *in vitro* (Fig. 7) and *in vivo* (Fig. 9). Our neurite arborization assay and neurite growth assay also demonstrates that the neurite branching was greater in a culture condition with GrowDex®-T and PODS®-BDNF (Fig. 7H). Ross et al. previously reported that unmyelinated SGNs tended to show multipolar morphology [112], and therefore, these multipolar neurites are more likely unmyelinated dendrites. Considering that our long-term aim is to generate a neuronal network connecting each of CI electrodes to extant SGNs, the larger dendritic tree that was shown in our study may, in fact, be pivotal in establishing the connection. A study in a feline retinal ganglion cell demonstrated that the shape and size of the receptive field are determined by the shape and size of underlying dendritic arborization [113]. They concluded that the larger the dendritic tree is, the larger the visual area over which they can receive the input. Computational studies also support this finding [114,115] If we translate this finding into the inner ear, the larger dendritic tree could receive more information from the CI electrode, which could potentially result in a lower threshold for electrical stimulation, a lower stimulation-current level requirement, and potentially higher spatial resolution (not so much for temporal resolution) of a biohybrid CI. Therefore, the higher arborization of neurites (unmyelinated dendrites) shown in this study may prove beneficial to our aim even though their shape is not bipolar. Further studies such as electrically-evoked ABR would give us more insight on this issue.

One of the limitations of this study was our immunohistochemistry. Due to the technical nature of AHNA, the antigen retrieval process was necessary, during which time our specimens were incubated under 120C° for 30 minutes. This treatment often distorted the thin-sliced specimens (Fig. 9). For future experiments, we recently developed and established lent-viral transfected fluorescent-positive hESC-derived ONPs to avoid antigen retrieval, improving image quality. Another limitation is that our ESC-derived ONP spheroids may have possessed molecular profiles similar, but not identical, to human SGNs. All of the markers we used in this study are not otic lineage specific. In addition, we have not performed any immunohistochemistry or qRT-PCR to distinguish our ONP spheroids from vestibular lineages. Once again, further functional studies such as electrically-evoked ABR would give us more insight into determining how much similarity in molecular profile is required for transplanted hESC-derived neurons to support a newly generated neuronal network within the inner ear.

On a technical note, hESC-derived ONP spheroid injections without the use of NFC hydrogel were not possible due to the constant backflow of perilymph from the scala tympani in the mice. The use of 0.375% or 0.5% of GrowDex®-T for injections did not allow any hESC-derived ONP spheroids to advance further in the scala tympani, presumably due to low viscosity and the stiffness of the gel. The use of 1% GrowDex®-T was chosen because its high viscosity and stiffness make injections feasible, allowed the hESC-derived ONPs to advance further into the scala tympani toward the mid-turn to secure placement, and displaced some transplanted ONPs in the scala media and the scala vestibuli. A future in vivo study may need to adjust the stiffness and viscosity of NFC hydrogel to place spheroids in the scala tympani and keep them localized despite the constant perilymphatic outflow.

5. Conclusions

Taken together, our data demonstrated that transplanted hESC-derived ONP spheroids survived, neuronally differentiated into otic neuronal lineages, and extended neurites toward the bony wall of the cochlea. Our data *in vitro* and *in vivo* presented here provide sufficient evidence that we have established a robust, reproducible protocol for *in vivo* transplantation of hESC-derived ONPs to the inner ear that may pave the way toward a next-generation “biohybrid” CI that combines the proven CI approach with hESC-replacement therapy [20]. Using our protocol to create an artificial stem cell niche in the inner ear using a 3D spheroid formation, NFC hydrogel for ECM, and a polyhedrin delivery system for the continuous provision of BDNF, it is once again possible to work toward integrating transplanted hESC-derived ONPs further into the inner ear as well as toward achieving functional auditory neurons generated from hESCs.

Supplementary Material

Refer to Web version on PubMed Central for supplementary material.

Acknowledgments

This work was supported by the American Otological Society Clinician Scientist Award (AJM), the Triological Society/American College of Surgeons Clinician Scientist Award (AJM), the Department of Otolaryngology of Northwestern University (AJM), the NIH (NIDCD) K08 Clinician Scientist Award K08DC13829-02 (AJM), and the Office of the Assistant Secretary of Defense of Health Affairs through the Hearing Restoration Research Program (Award #: RH170013:WU81XWUH-18-0712). Imaging work was performed at the Northwestern University Center for Advanced Microscopy, which is generously supported by NCI CCSG P30 CA060553 awarded to the Robert H. Lurie Comprehensive Cancer Center, for which we thank Peter Dluhy, Constadina Arvanitis, Ph.D., David Kirchenbuechler, Ph.D., and Wensheng (Wilson) Liu, M.D. Our rheological and viscoelastic experiments were performed in the Analytical bioNanoTechnology (ANTEC) Core Facility of the Simpson Querrey Institute at Northwestern University, which is supported by the Soft and Hybrid Nanotechnology Experimental (SHyNE) Resource (NSFECCS-1542205. We thank Jason Luo (Optic11 Life), Alexandra Kolot (ANTEC), Charles Bressan (ANTEC) for assistance in the use of a Piuma nadoindenter and Tony Kiuru, Ph.D., Markus Nuopponen, Ph.D., Lauri Paasonen, Ph.D. (UPM), Jonathan Sheard, Ph.D. (Sheard Biotech, Ltd.), and Christian Pernstich, Ph.D. (Cell Guidance System) for insightful comments and proofreading this manuscript.

8. References

[1]. Lin FR, Niparko JK, Ferrucci L, Hearing loss prevalence in the United States, Arch Otolaryngol Head Neck Surg. 171 (2014) 2011–2012. doi:10.1002/gps.2627.6.

[2]. Goman AM, Lin FR, Prevalence of hearing loss by severity in the United States, Am. J. Public Health. 106 (2016) 1820–1822. doi:10.2105/AJPH.2016.303299. [PubMed: 27552261]

[3]. Hinojosa R, Marion M, Histopathology of profound sensorineural deafness, Ann. N. Y. Acad. Sci 405 (1983) 459–484. doi:10.1111/j.1749-6632.1983.tb31662.x. [PubMed: 6575668]

[4]. Glueckert R, Bitsche M, Miller JM, Zhu Y, Prieskorn DM, Altschuler RA, Schrott-Fischer A, Deafferentiation-associated changes in afferent and efferent processes in the guinea pig cochlea and afferent regeneration with chronic intrascalar brain-derived neurotrophic factor and acidic fibroblast growth factor, J. Comp. Neurol 507 (2008) 1602–1621. doi:10.1002/cne. [PubMed: 18220258]

[5]. Spoendlin H, Factors inducing retrograde degeneration of the cochlear nerve, Ann. Otol. Rhinol. Laryngol 93 (1984) 76–82. doi:10.3109/00016487509124683. [PubMed: 6538394]

[6]. Finley CC, Wilson BS, White MW, Models of neural responsiveness to electrical stimulation, in: Cochlear Implant., 1990: pp. 55–96. doi:10.1007/978-1-4612-3256-8_5.

[7]. Briaire JJ, Frijns JHM, Field patterns in a 3D tapered spiral model of the electrically stimulated cochlea, Hear. Res 148 (2000) 18–30. doi:10.1016/S0378-5955(00)00104-0. [PubMed: 10978822]

[8]. Clark GM, The multi-channel cochlear implant: Multi-disciplinary development of electrical stimulation of the cochlea and the resulting clinical benefit, Hear. Res 322 (2014) 4–13. doi:10.1016/j.heares.2014.08.002. [PubMed: 25159273]

[9]. O'Leary SJ, Richardson RR, McDermott HJ, Principles of design and biological approaches for improving the selectivity of cochlear implant electrodes., J. Neural Eng 6 (2009) 055002 (epub). doi:10.1088/1741-2560/6/5/055002. [PubMed: 19721188]

[10]. Zimmermann CE, Burgess BJ, Nadol JB, Patterns of degeneration in the human cochlear nerve, Hear. Res 90 (1995) 192–201. doi:10.1016/0378-5955(95)00165-1. [PubMed: 8974997]

[11]. Suzuka Y, Schuknecht H, Retrograde cochlear neuronal degeneration in human subjects, Acta Otolaryngol. Suppl 450 (1988) 1–20. [PubMed: 3207012]

[12]. Oshima K, Shin K, Diensthuber M, Peng AW, Ricci AJ, Heller S, Mechanosensitive hair cell-like cells from embryonic and induced pluripotent stem cells., Cell. 141 (2010) 704–16. doi:10.1016/j.cell.2010.03.035. [PubMed: 20478259]

[13]. Oshima K, Suchert S, Blevins NH, Heller S, Curing hearing loss: Patient expectations, health care practitioners, and basic science., J. Commun. Disord 43 (2010) 311–8. doi:10.1016/j.jcomdis.2010.04.002. [PubMed: 20434163]

[14]. Rask-Andersen H, Liu W, Erixon E, Kinnefors A, Pfaller K, Schrott-Fischer A, Glueckert R, Human cochlea: Anatomical characteristics and their relevance for cochlear implantation, Anat. Rec 295 (2012) 1791–1811. doi:10.1002/ar.22599.

[15]. Chen W, Jongkamonwiwat N, Abbas L, Eshtan SJ, Johnson SL, Kuhn S, Milo M, Thurlow JK, Andrews PW, Marcotti W, Moore HD, Rivolta MN, Restoration of auditory evoked responses by human ES-cell-derived otic progenitors, Nature. 490 (2012) 278–282. doi:10.1038/nature11415. [PubMed: 22972191]

[16]. Geleoc GSG, Holt JR, Sound Strategies for Hearing Restoration, Science (80-.). 344 (2014) 1241062–1–1241062–8. doi:10.1126/science.1241062.

[17]. Staecker H, Kopke R, Malgrange B, Lefebvre P, Van de Water TR, NT-3 and/or BDNF therapy prevents loss of auditory neurons following loss of hair cells, Neuroreport. 7 (1996) 889–894. doi:10.1097/00001756-199603220-00011. [PubMed: 8724667]

[18]. Li H, Edin F, Hayashi H, Gudjonsson O, Danckwardt-Lilliestrm N, Engqvist H, Rask-Andersen H, Xia W, Guided growth of auditory neurons: bioactive particles towards gapless neural-electrode interface, Biomaterials. 122 (2017) 1–9. doi:10.1016/j.biomaterials.2016.12.020. [PubMed: 28107660]

[19]. Küçük B, Abe K, Ushiki T, Inuyama Y, Fukuda S, Ishikawa K, Microstructures of the bony modiolus in the human cochlea: a scanning electron microscopic study., J Electron Microsc (Tokyo). 40 (1991) 193–197. [PubMed: 1791403]

[20]. Roemer A, Köhl U, Majdani O, Klöß S, Falk C, Haumann S, Lenarz T, Kral A, Warnecke A, Biohybrid cochlear implants in human neurosensory restoration, Stem Cell Res. Ther (2016) 1–14. doi:10.1186/s13287-016-0408-y. [PubMed: 26729060]

[21]. Lutolf MP, Blau HM, Artificial Stem Cell Niches, Adv. Mater 21 (2009) 3255–3268. doi:10.1002/adma.200802582. [PubMed: 20882496]

[22]. Dimmeler S, Ding S, Rando TA, Trounson A, Translational strategies and challenges in regenerative medicine., Nat. Med 20 (2014) 814–21. doi:10.1038/nm.3627. [PubMed: 25100527]

[23]. Donnelly H, Salmeron-Sanchez M, Dalby MJ, Designing stem cell niches for differentiation and self-renewal, J. R. Soc. Interface 15 (2018). doi:10.1098/rsif.2018.0388.

[24]. Lane SW, Williams DA, Watt FM, Modulating the stem cell niche for tissue regeneration, Nat. Biotechnol 32 (2014) 795–803. doi:10.1038/nbt.2978. [PubMed: 25093887]

[25]. Reichardt LF, Neurotrophin-regulated signalling pathways, Philos. Trans. R. Soc. B Biol. Sci 361 (2006) 1545–1564. doi:10.1098/rstb.2006.1894.

[26]. Matsuoka AJ, Kondo T, Miyamoto RT, Hashino E, Enhanced survival of bone-marrow-derived pluripotent stem cells in an animal model of auditory neuropathy., Laryngoscope. 117 (2007) 1629–1635. doi:10.1097/MLG.0b013e31806bf282. [PubMed: 17632425]

[27]. Matsuoka AJ, Kondo T, Miyamoto RT, Hashino E, In vivo and in vitro characterization of bone marrow-derived stem cells in the cochlea., Laryngoscope. 116 (2006) 1363–1367. doi:10.1097/01.mlg.0000225986.18790.75. [PubMed: 16885736]

[28]. Corrales C, Pan L, Li H, Liberman MC, Heller S, Edge ASB, Engraftment and differentiation of embryonic stem cell–derived neural progenitor cells in the cochlear nerve trunk: Growth of processes into the organ of Corti, J. Neurobiol 66 (2006) 489–500. doi:10.1002/neu.

[29]. Nayagam BA, Backhouse SS, Cimenkaya C, Shepherd RK, Hydrogel limits stem cell dispersal in the deaf cochlea: Implications for cochlear implants, J. Neural Eng 9 (2012) 065001. doi:10.1088/1741-2560/9/6/065001. [PubMed: 23186887]

[30]. Kondo T, Matsuoka AJ, Shimomura A, Koehler KR, Chan RJ, Miller JM, Srour EF, Hashino E, Wnt signaling promotes neuronal differentiation from mesenchymal stem cells through activation of Tlx3., Stem Cells. 29 (2011) 836–846. doi:10.1002/stem.624. [PubMed: 21374761]

[31]. Hu Z, Ulfendahl M, The potential of stem cells for the restoration of auditory function in humans, Regen. Med 8 (2013) 309–318. doi:10.2217/rme.13.32. [PubMed: 23627825]

[32]. Takeda H, Hosoya M, Fujioka M, Saegusa C, Saeki T, Miwa T, Okano H, Minoda R, Engraftment of Human Pluripotent Stem Cell-derived Progenitors in the Inner Ear of Prenatal Mice, Sci. Rep 8 (2018) 1–10. doi:10.1038/s41598-018-20277-5. [PubMed: 29311619]

[33]. Rask-Andersen H, Schrott-Fischer A, Pfaller K, Glueckert R, Perilymph/modiolar communication routes in the human cochlea., Ear Hear. 27 (2006) 457–465. doi:10.1097/01.aud.0000233864.32183.81. [PubMed: 16957497]

[34]. Hosseinkhani M, Shirazi R, Rajaei F, Mahmoudi M, Mohammadi N, Abbasi M, Engineering of the embryonic and adult stem cell niches., Iran. Red Crescent Med. J 15 (2013) 83–92. doi:10.5812/ircmj.7541. [PubMed: 23682319]

[35]. Petrenko Y, Syková E, Kubinová Š, The therapeutic potential of three-dimensional multipotent mesenchymal stromal cell spheroids, Stem Cell Res. Ther 8 (2017) 94. doi:10.1186/s13287-017-0558-6. [PubMed: 28446248]

[36]. Ishikawa M, Ohnishi H, Skerleva D, Sakamoto T, Yamamoto N, Hotta A, Ito J, Nakagawa T, Transplantation of neurons derived from human iPS cells cultured on collagen matrix into guinea-pig cochleae., J. Tissue Eng. Regen. Med (2015) Epub ahead of print, DOI: 10.1002/term.2072. doi:10.1002/term.2072.

[37]. Jhala D, Vasita R, A review on extracellular matrix mimicking strategies for an artificial stem cell niche, Polym. Rev 55 (2015) 561–595. doi:10.1080/15583724.2015.1040552.

[38]. Gattazzo F, Urciuolo A, Bonaldo P, Extracellular matrix: A dynamic microenvironment for stem cell niche, Biochim. Biophys. Acta - Gen. Subj 1840 (2014) 2506–2519. doi:10.1016/j.bbagen.2014.01.010.

[39]. Hou L, Coller J, Natu V, Hastie TJ, Huang NF, Combinatorial extracellular matrix microenvironments promote survival and phenotype of human induced pluripotent stem cell-derived endothelial cells in hypoxia, Acta Biomater. 44 (2016) 188–199. doi:10.1016/j.actbio.2016.08.003. [PubMed: 27498178]

[40]. Bhattacharya M, Malinen MM, Lauren P, Lou YR, Kuisma SW, Kanninen L, Lille M, Corlu A, Guguen-Guillouzo C, Ikkala O, Laukkanen A, Urtti A, Yliperttula M, Nanofibrillar cellulose hydrogel promotes three-dimensional liver cell culture, J. Control. Release 164 (2012) 291–298. doi:10.1016/j.jconrel.2012.06.039. [PubMed: 22776290]

[41]. Paukkonen H, Ukkonen A, Szilvay G, Yliperttula M, Laaksonen T, Hydrophobin-nanofibrillated cellulose stabilized emulsions for encapsulation and release of BCS class II drugs, Eur. J. Pharm. Sci 100 (2017) 238–248. doi:10.1016/j.ejps.2017.01.029.

[42]. Lou YR, Kanninen L, Kuisma T, Niklander J, Noon LA, Burks D, Urtti A, Yliperttula M, The use of nanofibrillar cellulose hydrogel as a flexible three-dimensional model to culture human pluripotent stem cells, Stem Cells Dev. 23 (2014) 380–392. doi:10.1089/scd.2013.0314. [PubMed: 24188453]

[43]. Märtson M, Viljanto J, Hurme T, Laippala P, Saukko P, Is cellulose sponge degradable or stable as implantation material? An in vivo subcutaneous study in the rat, Biomaterials. 20 (1999) 1989–1995. doi:10.1016/S0142-9612(99)00094-0.

[44]. Miyamoto T, Takahashi S, Ito H, Inagak H, Noishiki Y, Tissue biocompatibility of cellulose and its derivatives., J Biomed Mater Res. 23 (1989) 125–133. [PubMed: 2708402]

[45]. Baseri B, Choi JJ, Deffieux T, Samiotaki M, Tung Y-S, Olumolade O, Small SA, Morrison III B, Konofagou EE, Activation of signaling pathways following localized delivery of systemically-administered neurotrophic factors across the blood-brain barrier using focused ultrasound and microbubbles, Phys Med Biol. 57 (2012) N65–N81. doi:10.1126/scitranslmed.3008882.Plasmodium. [PubMed: 22407323]

[46]. Mori H, Ito R, Nakazawa H, Sumida M, Matsubara F, Minobe Y, Expression of Bombyx mori cytoplasmic polyhedrosis virus polyhedrin in insect cells by using a baculovirus expression vector, and its assembly into polyhedra, J. Gen. Virol 74 (1993) 99–102. doi:10.1099/0022-1317-74-1-99. [PubMed: 8423453]

[47]. Mori H, Minobe Y, Sasaki T, Kawase S, Nucleotide sequence of the polyhedrin gene of Bombyx mori cytoplasmic polyhedrosis virus A strain with nuclear localization of polyhedra., J. Gen. Virol 70 (Pt 7) (1989) 1885–1888. [PubMed: 2661724]

[48]. Ikeda K, Nagaoka S, Winkler S, Kotani K, Yagi H, Nakanishi K, Miyajima S, Kobayashi J, Mori H, Molecular Characterization of Bombyx mori Cytoplasmic Polyhedrosis Virus Genome Segment 4, J. Virol 75 (2001) 988–995. doi:10.1128/jvi.75.2.988-995.2001. [PubMed: 11134312]

[49]. Ramekers D, Versnel H, Grolman W, Klis SFL, Neurotrophins and their role in the cochlea., Hear. Res 288 (2012) 19–33. doi:10.1016/j.heares.2012.03.002. [PubMed: 22465680]

[50]. Bailey EM, Green SH, Postnatal Expression of Neurotrophic Factors Accessible to Spiral Ganglion Neurons in the Auditory System of Adult Hearing and Deafened Rats, J. Neurosci 34 (2014) 13110–13126. doi:10.1523/JNEUROSCI.1014-14.2014. [PubMed: 25253857]

[51]. Green SH, Bailey E, Wang Q, Davis RL, The Trk A B, C's of neurotrophins in the cochlea., Anat. Rec. (Hoboken) 295 (2012) 1877–1895. doi:10.1002/ar.22587. [PubMed: 23044862]

[52]. Golub JS, Tong L, Ngyuen TB, Hume CR, Palmiter RD, Rubel EW, Stone JS, Hair cell replacement in adult mouse utricles after targeted ablation of hair cells with diphtheria toxin, J Neurosci. 32 (2013) 15093–15105. doi:10.1523/JNEUROSCI.1709-12.2012.Hair.

[53]. Tong L, Strong MK, Kaur T, Juiz JM, Oesterle EC, Hume C, Warchol ME, Palmiter RD, Rubel EW, Selective deletion of cochlear hair cells causes rapid age-dependent changes in spiral ganglion and cochlear nucleus neurons, J. Neurosci 35 (2015) 7878–7891. doi:10.1523/JNEUROSCI.2179-14.2015. [PubMed: 25995473]

[54]. Kurioka T, Lee MY, Heeringa AN, Beyer LA, Swiderski DL, Kanicki AC, Kabara LL, Dolan DF, Shorea SE, Raphael Y, Selective hair cell ablation and noise exposure lead to different patterns of changes in the cochlea and the cochlear nucleus, Neuroscience. 332 (2016) 242–257. doi:10.1016/j.physbeh.2017.03.040. [PubMed: 27403879]

[55]. Tong L, Strong MK, Kaur T, Juiz JM, Oesterle EC, Hume C, Warchol ME, Palmiter RD, Rubel EW, Selective Deletion of Cochlear Hair Cells Causes Rapid Age-Dependent Changes in Spiral Ganglion and Cochlear Nucleus Neurons, J. Neurosci 35 (2015) 7878–7891. doi:10.1523/JNEUROSCI.2179-14.2015. [PubMed: 25995473]

[56]. Matsuoka AJ, Morrissey ZD, Zhang C, Homma K, Belmadani A, Miller CA, Chadly DM, Kobayashi S, Edelbrock AN, Tanaka-Matakatsu M, Whitlon DS, Lyass L, McGuire TL, Stupp SI, Kessler JA, Directed differentiation of human embryonic stem cells toward placode-derived spiral ganglion-like sensory neurons., Stem Cells Transl. Med 6 (2017) 923–936. doi:10.1002/sctm.16-0032. [PubMed: 28186679]

[57]. Burry RW, Controls for immunocytochemistry: An update, J. Histochem. Cytochem 59 (2011) 6–12. doi:10.1369/jhc.2010.956920. [PubMed: 20852036]

[58]. Saper CB, Sawchenko PE, Magic peptides, magic antibodies: Guidelines for appropriate controls for immunohistochemistry, J. Comp. Neurol 465 (2003) 161–163. doi:10.1002/cne.10858. [PubMed: 12949777]

[59]. Golub JS, Tong L, Ngyuen TB, Hume CR, Palmiter RD, Rubel EW, Stone JS, Hair Cell Replacement in Adult Mouse Utricles after Targeted Ablation of Hair Cells with Diphtheria Toxin, J. Neurosci 32 (2012) 15093–15105. doi:10.1523/JNEUROSCI.1709-12.2012. [PubMed: 23100430]

[60]. Schindelin J, Arganda-Carreras I, Frise E, Kaynig V, Longair M, Pietzsch T, Preibisch S, Rueden C, Saalfeld S, Schmid B, Tinevez JY, White DJ, Hartenstein V, Eliceiri K, Tomancak P, Cardona A, Fiji: An open-source platform for biological-image analysis, Nat. Methods 9 (2012) 676–682. doi:10.1038/nmeth.2019. [PubMed: 22743772]

[61]. Abercombie M, Estimation of nuclear population from microtome sections., Anat Rec. 94 (1946) 239–247. [PubMed: 21015608]

[62]. Coggeshall RE, Lekan HA, Methods for determining numbers of cells and synapses: A case for more uniform standards of review, J. Comp. Neurol 364 (1996) 6–15. doi:10.1002/(SICI)1096-9861(19960101)364:1<6::AID-CNE2>3.0.CO;2-9. [PubMed: 8789272]

[63]. Matsuoka AJ, Sayed ZA, Stephanopoulos N, Berns EJ, Wadhwani AR, Morrissey ZD, Chadly DM, Kobayashi S, Edelbrock AN, Mashimo T, Miller CA, McGuire TL, Stupp SI, Kessler JA, Creating a stem cell niche in the inner ear using self-assembling peptide amphiphiles, PLoS One. 12 (2017) e0190150. doi:10.1371/journal.pone.0190150. [PubMed: 29284013]

[64]. Herburger K, Holzinger A, Aniline Blue and Calcofluor White Staining of Callose and Cellulose in the Streptophyte Green Algae Zygnema and Klebsormidium, Bio-Protocol. 6 (2016) 6–10. doi:10.21769/bioprotoc.1969.

[65]. Yuan X, Zhang H, jie Wei Y, shou Hu S, Embryonic stem cell transplantation for the treatment of myocardial infarction: Immune privilege or rejection, Transpl. Immunol 18 (2007) 88–93. doi:10.1016/j.trim.2007.05.003. [PubMed: 18005850]

[66]. Blainey P, Krzywinski M, Altman N, Points of significance: Replication, Nat. Methods 11 (2014) 879–880. doi:10.1038/nmeth.3091. [PubMed: 25317452]

[67]. Tsvetkov D, Kolpakov E, Kassmann M, Schubert R, Gollasch M, Distinguishing Between Biological and Technical Replicates in Hypertension Research on Isolated Arteries, Front. Med 6 (2019) 1–8. doi:10.3389/fmed.2019.00126.

[68]. R Development Core Team., R: A Language and Environment for Statistical Computing, (2016).

[69]. Anniko M, Arnold W, Stigbrand T, Strom A, The Human Spiral Ganglion, ORL. 57 (1995) 68–77. [PubMed: 7537360]

[70]. Chen W, Cacciabue-Rivolta DI, Moore HD, Rivolta MN, The human fetal cochlea can be a source for auditory progenitors/stem cells isolation., Hear. Res 233 (2007) 23–9. doi:10.1016/j.heares.2007.06.006. [PubMed: 17646067]

[71]. Jones JM, Warchol ME, Expression of the Gata3 transcription factor in the acoustic ganglion of the developing avian inner ear., J. Comp. Neurol 516 (2009) 507–518. doi:10.1002/cne.22128. [PubMed: 19673002]

[72]. Raft S, Koundakjian EJ, Quinones H, Jayasena CS, V Goodrich L, Johnson JE, Segil N, Groves AK, Cross-regulation of Ngn1 and Math1 coordinates the production of neurons and sensory hair cells during inner ear development., Development. 134 (2007) 4405–15. doi:10.1242/dev.009118. [PubMed: 18039969]

[73]. Gálvez H, Abelló G, Giraldez F, Signaling and Transcription Factors during Inner Ear Development: The Generation of Hair Cells and Otic Neurons, Front. Cell Dev. Biol 5 (2017) 1–13. doi:10.3389/fcell.2017.00021. [PubMed: 28184371]

[74]. Bouchard M, de Caprona D, Busslinger M, Xu P, Fritzsch B, Pax2 and Pax8 cooperate in mouse inner ear morphogenesis and innervation., BMC Dev. Biol 10 (2010) 89. doi:10.1186/1471-213X-10-89. [PubMed: 20727173]

[75]. McCarroll MN, Lewis ZR, Culbertson MD, Martin BL, Kimelman D, V Nechiporuk A, Graded levels of Pax2a and Pax8 regulate cell differentiation during sensory placode formation., Development. 139 (2012) 2740–50. doi:10.1242/dev.076075. [PubMed: 22745314]

[76]. Kondo T, Sheets PL, Zopf DA, Aloor HL, Cummins TR, Chan RJ, Hashino E, Tlx3 exerts context-dependent transcriptional regulation and promotes neuronal differentiation from embryonic stem cells., Proc. Natl. Acad. Sci. U. S. A 105 (2008) 5780–5785. doi:10.1073/pnas.0708704105. [PubMed: 18391221]

[77]. Gunewardene N, Van Bergen N, Crombie D, Needham K, Dottori M, Nayagam BA, Directing human induced pluripotent stem cells into a neurosensory lineage for auditory neuron replacement., Biores. Open Access. 3 (2014) 162–75. doi:10.1089/biores.2014.0019. [PubMed: 25126480]

[78]. Liu Q, Lei L, Yu T, Jiang T, Kang Y, Effect of Brain-Derived Neurotrophic Factor on the Neurogenesis and Osteogenesis in Bone Engineering, Tissue Eng. - Part A. 24 (2018) 1283–1292. doi:10.1089/ten.tea.2017.0462. [PubMed: 29490590]

[79]. Lee KS, Zhou W, Scott-McKean JJ, Emmerling KL, Cai G, Krah DL, Costa AC, Freed CR, Levin MJ, Human sensory neurons derived from induced pluripotent stem cells support varicella-zoster virus infection., PLoS One. 7 (2012) e53010. doi:10.1371/journal.pone.0053010. [PubMed: 23285249]

[80]. Grocott T, Tambalo M, Streit A, The peripheral sensory nervous system in the vertebrate head: a gene regulatory perspective., Dev. Biol 370 (2012) 3–23. doi:10.1016/j.ydbio.2012.06.028. [PubMed: 22790010]

[81]. Pieper M, Eagleson GW, Wosniok W, Schlosser G, Origin and segregation of cranial placodes in Xenopus laevis., Dev. Biol 360 (2011) 257–75. doi:10.1016/j.ydbio.2011.09.024. [PubMed: 21989028]

[82]. Betancur P, Sauka-spengler T, Bronner M, A Sox10 enhancer element common to the otic placode and neural crest is activated by tissue-specific paralogs, Development. 3698 (2011) 3689–3698. doi:10.1242/dev.057836.

[83]. Er JC, Leong C, Teoh CL, Yuan Q, Merchant P, Dunn M, Sulzer D, Sames D, Bhinge A, Kim D, Kim SM, Yoon MH, Stanton LW, Je SH, Yun SW, Chang YT, Neuo: A fluorescent chemical probe for live neuron labeling, Angew. Chemie - Int. Ed 54 (2015) 2442–2446. doi:10.1002/anie.201408614.

[84]. Hafidi A, Fellous A, Ferhat L, Romand M-R, Romand R, Developmental differentiation of MAP2 expression in the central versus the peripheral and efferent projections of the inner ear, J. Comp. Neurol 323 (1992) 423–431. doi:10.1002/cne.903230309. [PubMed: 1281171]

[85]. Chandrasekaran A, Avci HX, Ochalek A, Rösingh LN, Molnár K, László L, Bellák T, Téglási A, Pesti K, Mike A, Phanthong P, Bíró O, Hall V, Kitiyanant N, Krause KH, Kobolák J, Dinnyés A, Comparison of 2D and 3D neural induction methods for the generation of neural progenitor cells from human induced pluripotent stem cells, Stem Cell Res. 25 (2017) 139–151. doi:10.1016/j.scr.2017.10.010. [PubMed: 29128818]

[86]. Koehler KR, Hashino E, 3D mouse embryonic stem cell culture for generating inner ear organoids., Nat Protoc. 9 (2014) 1229–1244. doi:10.1038/nprot.2014.100. [PubMed: 24784820]

[87]. Koehler KR, Nie J, Longworth-Mills E, Liu XP, Lee J, Holt JR, Hashino E, Generation of inner ear organoids containing functional hair cells from human pluripotent stem cells, Nat. Biotechnol 35 (2017) 583–589. doi:10.1038/nbt.3840. [PubMed: 28459451]

[88]. Lu CC, Appler JM, Houseman EA, V Goodrich L, Developmental profiling of spiral ganglion neurons reveals insights into auditory circuit assembly., J. Neurosci 31 (2011) 10903–10918. doi:10.1523/JNEUROSCI.2358-11.2011. [PubMed: 21795542]

[89]. Incesulu A, Nadol JB, Correlation of acoustic threshold measures and spiral ganglion cell survival in severe to profound sensorineural hearing loss: implications for cochlear implantation., Ann. Otol. Rhinol. Laryngol 107 (1998) 906–11. doi:10.1177/000348949810701102. [PubMed: 9823838]

[90]. Wilson BS, Dorman MF, Woldorff MG, Tucci DL, Cochlear implants matching the prosthesis to the brain and facilitating desired plastic changes in brain function., Prog. Brain Res 194 (2011) 117–29. doi:10.1016/B978-0-444-53815-4.00012-1. [PubMed: 21867799]

[91]. Incesulu A, Nadol JB, Correlation of acoustic threshold measures and spiral ganglion cell survival in severe to profound sensorineural hearing loss: implications for cochlear implantation., Ann. Otol. Rhinol. Laryngol 107 (1998) 906–11. doi:10.1177/000348949810701102. [PubMed: 9823838]

[92]. Nadol JB, Patterns of neural degeneration in the human cochlea and auditory nerve: implications for cochlear implantation., Otolaryngol. Head. Neck Surg 117 (1997) 220–228. doi:10.1016/S0194-5998(97)70178-5. [PubMed: 9334769]

[93]. Nadol JB, Comparative anatomy of the cochlea and auditory nerve in mammals, Hear. Res 34 (1988) 253–266. doi:10.1016/0378-5955(88)90006-8. [PubMed: 3049492]

[94]. Nadol JB, Degeneration of cochlear neurons as seen in the spiral ganglion of man, Hear. Res 49 (1990) 141–154. doi:10.1016/0378-5955(90)90101-T. [PubMed: 2292494]

[95]. Matsuoka AJ, Kondo T, Miyamoto RT, Hashino E, In Vivo and In Vitro Characterization of Bone Marrow-Derived Stem Cells in the Cochlea, Laryngoscope. 116 (2006) 1363–1367. doi:10.1097/01.mlg.0000225986.18790.75. [PubMed: 16885736]

[96]. Ginis I, Luo Y, Miura T, Thies S, Brandenberger R, Gerecht-Nir S, Amit M, Hoke A, Carpenter MK, Itskovitz-Eldor J, Rao MS, Differences between human and mouse embryonic stem cells, Dev. Biol 269 (2004) 360–380. doi:10.1016/j.ydbio.2003.12.034. [PubMed: 15110706]

[97]. Barclay M, Ryan AF, Housley GD, Type I vs type II spiral ganglion neurons exhibit differential survival and neuritogenesis during cochlear development, Neural Dev. 6 (2011) 33. doi:10.1186/1749-8104-6-33. [PubMed: 21989106]

[98]. Perny M, Ting C-C, Kleinlogel S, Senn P, Roccio M, Generation of Otic Sensory Neurons from Mouse Embryonic Stem Cells in 3D Culture, Front. Cell. Neurosci 11 (2017) 1–12. doi:10.3389/fncel.2017.00409. [PubMed: 28154525]

[99]. Laurén P, Lou YR, Raki M, Urtti A, Bergström K, Yliperttula M, Technetium-99m-labeled nanofibrillar cellulose hydrogel for in vivo drug release, Eur. J. Pharm. Sci 65 (2014) 79–88. doi:10.1016/j.ejps.2014.09.013.

[100]. Miron-Mendoza M, Seemann J, Grinnell F, The differential regulation of cell motile activity through matrix stiffness and porosity in three dimensional collagen matrices, Biomaterials. 31 (2010) 6425–6435. doi:10.1016/j.biomaterials.2010.04.064. [PubMed: 20537378]

[101]. Groebe K, Mueller-Klieser W, On the relation between size of necrosis and diameter of tumor spheroids, Int. J. Radiat. Oncol. Biol. Phys 34 (1996) 395–401. doi:10.1016/0360-3016(95)02065-9. [PubMed: 8567341]

[102]. Praetorius M, Vicario I, Schimmang T, Efficient transfer of embryonic stem cells into the cochlea via a non-invasive vestibular route, Acta Otolaryngol. 128 (2008) 720–723. doi:10.1080/00016480701714236. [PubMed: 18568511]

[103]. Lee MY, Hackelberg S, Green KL, Lunghamer KG, Kurioka T, Loomis BR, Swiderski DL, Duncan RK, Raphael Y, Survival of human embryonic stem cells implanted in the Guinea pig auditory epithelium, Sci. Rep 7 (2017) 1–12. doi:10.1038/srep46058. [PubMed: 28127051]

[104]. Boyd AS, Higashi Y, Wood KJ, Transplanting stem cells: Potential targets for immune attack. Modulating the immune response against embryonic stem cell transplantation, Adv. Drug Deliv. Rev 57 (2005) 1944–1969. doi:10.1016/j.addr.2005.08.004. [PubMed: 16289432]

[105]. Drukker M, Katchman H, Katz G, Even-Tov Friedman S, Shezen E, Hornstein E, Mandelboim O, Reisner Y, Benvenisty N, Human Embryonic Stem Cells and Their Differentiated Derivatives Are Less Susceptible to Immune Rejection Than Adult Cells, Stem Cells. 24 (2006) 221–229. doi:10.1634/stemcells.2005-0188. [PubMed: 16109762]

[106]. Drukker M, Katz G, Urbach A, Schuldiner M, Markel G, Itskovitz-Eldor J, Reubinoff B, Mandelboim O, Benvenisty N, Characterization of the expression of MHC proteins in human embryonic stem cells, Proc. Natl. Acad. Sci. U. S. A 99 (2002) 9864–9869. doi:10.1073/pnas.142298299. [PubMed: 12114532]

[107]. Li L, BAROJA ML, MAJUMDAR ANISH, CHADWICK K, ROULEAU A, GALLACHER L, FERBER I, LEBKOWSKI J, MARTIN T, MADRENAS J, BHATIA M, Human Embryonic Stem Cells Possess Immune-Privileged Properties, Stem Cells. 22 (2004) 448–456. [PubMed: 15277692]

[108]. Harris JP, Ryan AF, Fundamental immune mechanisms of the brain and inner ear., Otolaryngol. Head. Neck Surg 112 (1995) 639–53. http://www.ncbi.nlm.nih.gov/pubmed/7777346. [PubMed: 7777346]

[109]. Louveau A, Harris TH, Kipnis J, Revisiting the concept of CNS immune privilege., Trends Immunol. 36 (2016) 569–577. doi:10.1016/j.it.2015.08.006.Revisiting.

[110]. Fujioka M, Okano H, Ogawa K, Inflammatory and immune responses in the cochlea: Potential therapeutic targets for sensorineural hearing loss, Front. Pharmacol 5 (2014) 1–5. doi:10.3389/fphar.2014.00287. [PubMed: 24478702]

[111]. Jowkarderis L, Van De Ven TGM, Mesh size analysis of cellulose nanofibril hydrogels using solute exclusion and PFG-NMR spectroscopy, Soft Matter. 11 (2015) 9201–9210. doi:10.1039/c5sm01752a. [PubMed: 26417984]

[112]. Ross MD, Burkel W, Multipolar neurons in the spiral ganglion of the rat, Acta Otolaryngol. 76 (1973) 381–394. doi:10.3109/00016487309121526. [PubMed: 4773103]

[113]. Peichl L, Wässle H, The structural correlate of the receptive field centre of alpha ganglion cells in the cat retina., J. Physiol 341 (1983) 309–324. doi:10.1113/jphysiol.1983.sp014807. [PubMed: 6620182]

[114]. Elias JG, Artificial Dendritic Trees, Neural Comput. 5 (1993) 648–664. doi:10.1162/neco.1993.5.4.648.

[115]. London M, Häusser M, Dendritic Computation, Annu. Rev. Neurosci 28 (2005) 503–532. doi:10.1146/annurev.neuro.28.061604.135703. [PubMed: 16033324]

Statement of Significance

Inner ear regeneration utilizing human embryonic stem cell-derived otic neuronal progenitors (hESC-derived ONPs) has remarkable potential for treating sensorineural hearing loss. However, the local environment of the inner ear requires a suitable stem cell niche to allow hESC-derived ONP engraftment as well as neuronal differentiation. To overcome this obstacle, we utilized three-dimensional spheroid formation (direct contact), nanofibrillar cellulose hydrogel (extracellular matrix), and a neurotrophic factor delivery system to artificially create a stem cell niche *in vitro* and *in vivo*. Our *in vitro* and *in vivo* data presented here provide sufficient evidence that we have established a robust, reproducible protocol for *in vivo* transplantation of hESC-derived ONPs to the inner ear.

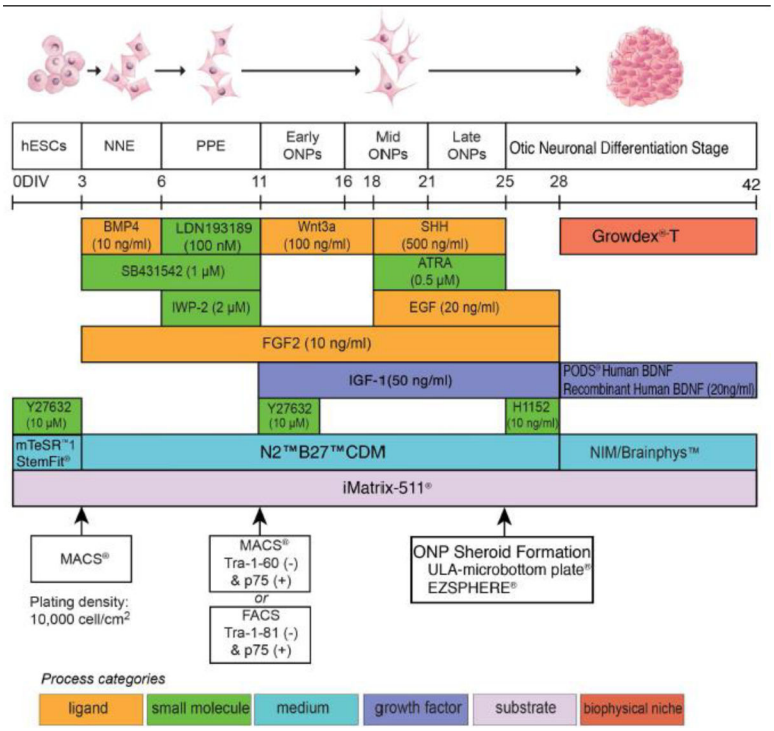

Figure 1.

Illustrative summary of a stepwise treatment protocol for deriving an otic neuronal lineage from undifferentiated H1, H7, and H9 human embryonic stem cells lines. Developmental stages are shown at the top, above a timeline, and key treatments are shown below, using color-coded bars. Abbreviations: D: days; NNE: nonneuronal ectoderm; PPE: preplacodal ectoderm; ONP: otic neuronal progenitor; BMP4: bone morphogenetic protein 4; SHH: Sonic hedgehog; ATRA: all-trans retinoic acid; EGF: epidermal growth factor; BDNF: brain-derived neurotrophic factor; NT3: neurotrophin 3; IGF-1: insulin-like growth factor 1; FGF2: fibroblast growth factor 2; CDM: chemically-defined medium; NIM: neural induction medium; MACS: magnetic-activated cell sorting; FACS: fluorescence-activated cell sorting; p75: low-affinity neurotrophin receptor ($p75^{NTR}$). This protocol is adapted from Matsuoka *et. al.*, 2017 and 2018.

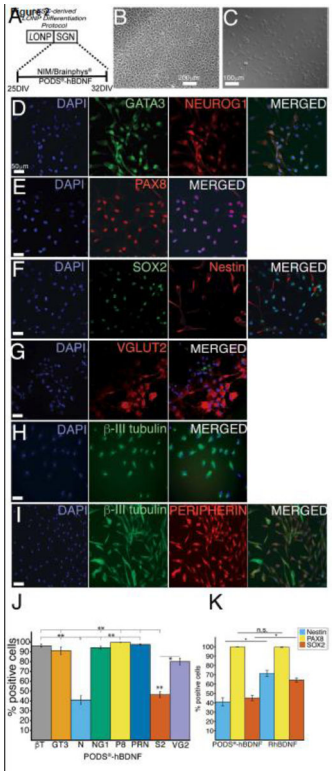

Figure 2.

Assessment of induction of an otic neuronal lineage from late-stage ONPs. **(A):** A stepwise treatment for an otic neuronal lineage induction. On day 25, PODS®-hBDNF treatment was started in NIM for 7 days. D: days. **(B):** Phase-contrast photomicrographs of hESC-derived late-stage ONPs. **(C):** Phase-contrast photomicrographs of hESC-derived ONPs treated with PODS®-hBDNF for seven days. **(D–I):** Immunocytochemistry of hESC-derived late-stage ONPs treated with PODS®-hBDNF in NIM/Brainphys™ shows expression of various otic neuronal markers: GATA3, NEUROG1, PAX8, SOX2, nestin, VGLUT2, β-III tubulin, and peripherin. **(J):** Quantification of the otic neuronal markers for % positivity (n = 3) on hESC-derived late-stage ONPs treated with PODS®-hBDNF for seven days. BT: β-III tubulin; GT3: GATA3; N: nestin; NG1: neurogenin 1; P8: PAX8; PRN: peripherin; S2: SOX2; and VG2: VGLUT2. **(K):** Quantification of % positive staining for nestin, PAX8, and SOX2 on PODS®-hBDNF and RhBDNF treated cells. *p <0.05, ** p < 0.01 by one-way ANOVA with Tukey's *post-hoc* test. n.s.: not statistically significant.

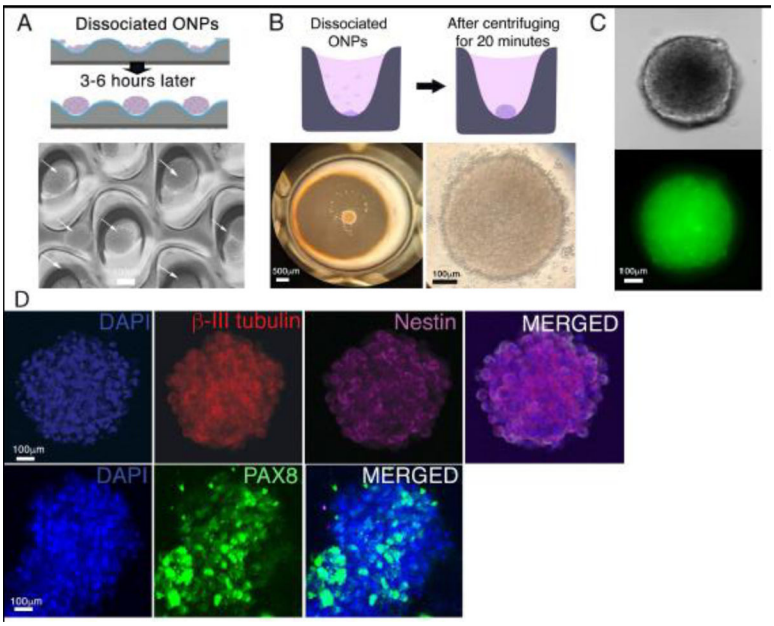

Figure 3.

Generation of hESC-derived ONP spheroids. **(A):** A schematic diagram of forming hESC-derived late-stage ONP spheroids using an EZSHPERE® plate (upper row) and a phase-contrast photomicrograph of individual spheroids (see white arrow) within the plate (bottom row). **(B):** A schematic diagram of forming hESC-derived ONP spheroids using a 96-well Clear Round Bottom Ultra-Low Attachment Microplate® (upper row) and a low-power (left bottom row) and high-power (right bottom row) phase-contrast photomicrograph of a spheroid within the plate. **(C):** A phase-contrast (upper row) and an epifluorescence (bottom row) photomicrographic image of a hESC-derived ONP spheroid stained with NeuroFluor™ NeuO. **(D):** Immunocytochemistry on a hESC-derived ONP spheroid that was cultured for seven days with 800,000 of PODS®-hBDNF. The spheroid was stained for β-III tubulin, nestin (upper row), and PAX8 (lower row).

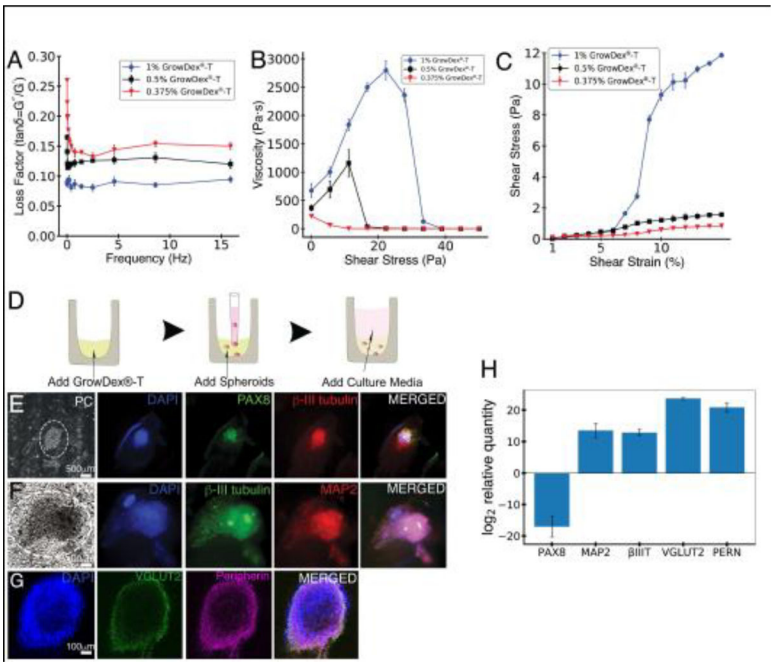

Figure 4.

Rheological characterization of GrowDex®-T and hESC-derived ONP spheroids cultured with GrowDex®-T**. (A):** Frequency sweep (viscoelasticity) of three different concentrations (1%, 0.5%, and 0.375%) of GrowDex®-T (n = 3)**. (B):** Influence of shear stress on the viscosity of three different concentrations (1%, 0.5%, and 0.375%) of GrowDex®-T (n = 3). **(C):** Strain sweep (stress-strain curve) of three different concentrations (1%, 0.5% and 0.375%) of GrowDex®-T. Shear modulus of 1%, 0.5% and 0.375% GrowDex®-T is plotted as a function of shear strain (n = 3). **(D):** Schematic figure of hESC-derived ONP spheroids cultured in GrowDex®-T. **(E–G):** Neuronal marker expressions of PAX8, β-III tubulin, MAP2, VGLUT2, peripherin and phase-contrast of hESC-derived ONP spheroids cultured with 0.375% GrowDex®-T. **(H):** Quantitative real-time PCR (qRT-PCR) on hESC-derived ONP spheroids cultured with 0.375% GrowDex®-T and 800,000 of PODS®-hBDNF relative to hESC-derived ONP spheroids cultured in Brainphys™ with 20 ng/mL of recombinant BDNF.

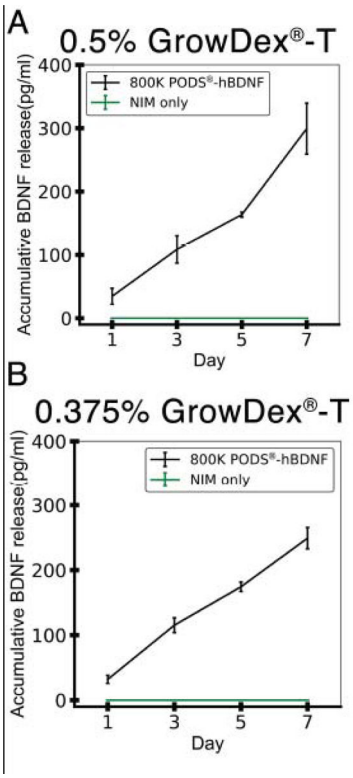

Figure 5.

Accumulative release kinetics of BDNF from PODS®-hBDNF and from a hESC-derived ONP spheroid cultured in NIM. **(A):** BDNF release profile of 800,000 PODS®-hBDNF in 0.5% GrowDex®-T over seven days. **(B):** BDNF release profile of 800,000 PODS®-hBDNF in 0.375% GrowDex®-T over seven days. In both **(A)** and **(B)**, accumulative release kinetic of BNNF from a hESC-derived ONP spheroid cultured in NIM is also plotted in a green line as a control.

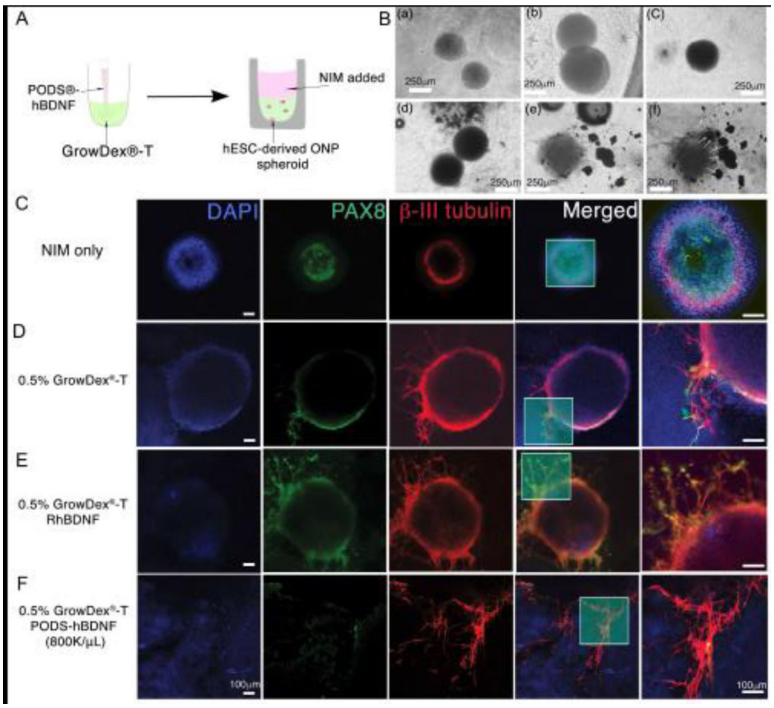

Figure 6.

Immunocytochemistry of hESC-derived ONP spheroids that were cultured with 0.5% GrowDex®-T *in vitro*. **(A):** Schematic diagram of PODS®-hBDNF and GrowDex®-T mixture with hESC-derived ONPs spheroids *in vitro*. **(B):** A phase-contrast photomicrograph of hESC-derived ONP spheroids cultured with GrowDex®-T (gray background) and/or PODS®-hBDNF (shown in black). Human ESC-derived ONP spheroids that were cultured with 1% GrowDex®-T for 24 hours (a), 48 hours (b), and 72 hours (c), respectively. Human ESC-derived ONP spheroids that were cultured with 1% GrowDex®-T and 800,000/μL of PODS®-hBDNF for 24 hours (d), 48 hours (e), and 72 hours (f), respectively. **(C):** Immunocytochemistry of hESC-derived ONP spheroids cultured in NIM for 7 days. **(D):** Immunocytochemistry of hESC-derived ONP spheroids cultured in 0.5% GrowDex®-T for seven days. **(E):** Immunocytochemistry of hESC-derived ONP spheroids cultured in 0.5% GrowDex®-T with 20 ng/mL of RhBDNF for seven days. **(F):** Immunocytochemistry of hESC-derived ONP spheroids cultured in 0.5% GrowDex®-T with 800,000 of PODS®-hBDNF for 7 days.

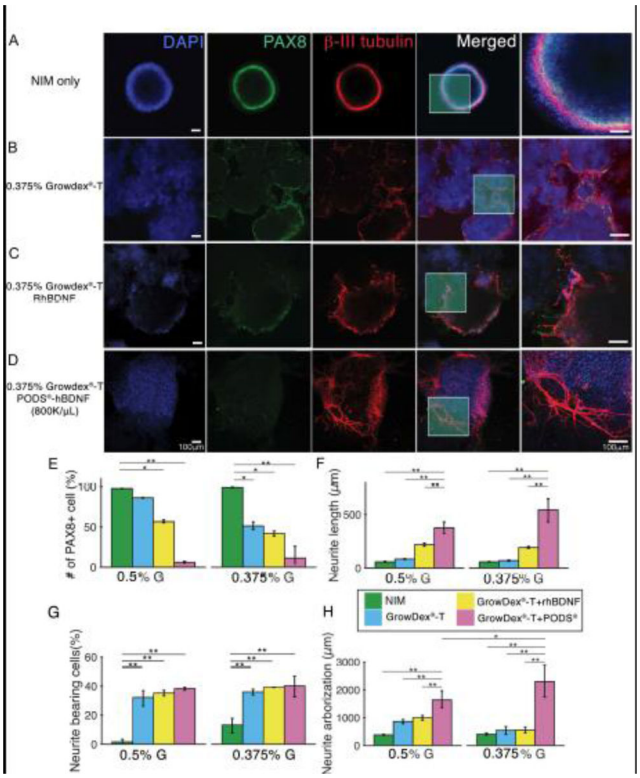

Figure 7.

Immunocytochemistry of hESC-derived ONP spheroids cultured with 0.375% GrowDex®-T *in vitro*. **(A):** Immunocytochemistry of hESCs-derived ONPs spheroids cultured in NIM for seven days. **(B):** Immunocytochemistry of hESC-derived ONP spheroids cultured in 0.375% GrowDex®-T for seven days. **(C):** Immunocytochemistry of hESC-derived ONP spheroids cultured in 0.375% GrowDex®-T with 20 ng/mL of RhBDNF for seven days. **(D):** Immunocytochemistry of hESC-derived ONP spheroids cultured in 0.375% GrowDex®-T with 800,000 of PODS®-hBDNF for seven days. **(E):** Quantification of positive staining for PAX8 based on immunocytochemistry in hESC-derived ONP spheroids. **(F):** Quantification of neurite length arising from hESC-derived ONP spheroids (n = 3). **(G):** Quantification of neurite bearing analysis. **(H):** Quantification of neurite arborization analysis. *$p < 0.05$, ** $p < 0.01$, *** $p < 0.001$ by one-way ANOVA with Tukey's *post-hoc* test.

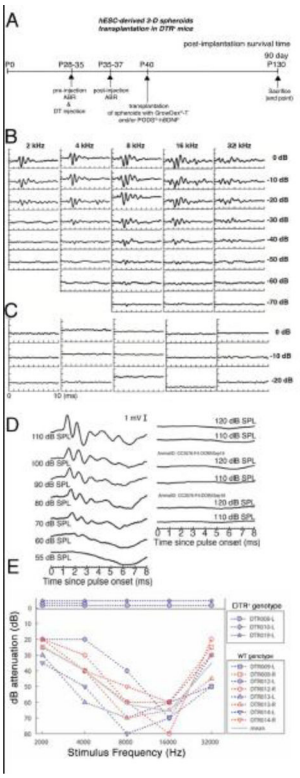

Figure 8.

In vivo hESC-derived ONP spheroid transplantation in the DTR mouse cochlea. **(A):** A schematic diagram of experimental design for *in vivo* hESC-derived ONP spheroid transplantation. **(B):** Tone-burst-evoked ABR assessment of a WT mouse. **(C):** Tone-burst-evoked ABR assessment of a DTR mouse. **(D):** Click-evoked ABR assessment of WT mouse (left column) and DTR mouse (right column). **(E):** ABR audiograms for 3 DTR and 8 WT mouse ears, with mean values for the latter shown with the gray line. Levels are expressed in terms of attenuation, with sound pressure levels at 0 dB ranging from 105 to 120 dB SPL. Thresholds were based upon visual detection of a response above the noise floor. No ABRs were detected for the three DTR mice (data plotted above the 0 dB line).

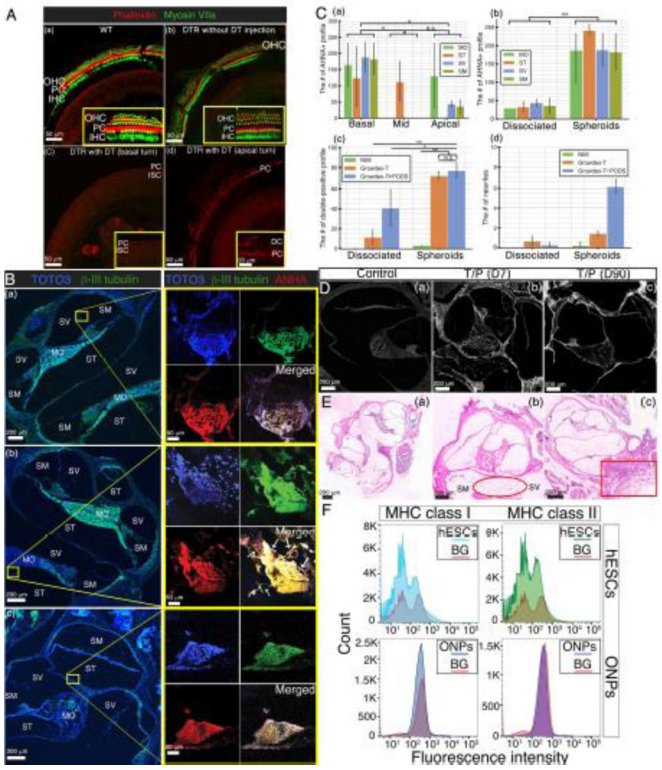

Figure 9. (A):

Immunohistochemistry of the DTR mouse cochlea. Confocal fluorescence imaged of phalloidin (red) and myosin VIIa (green) in the whole mounted auditory epithelium. (a) A wild type cochlea (control) shows a single row of IHCs and three rows of OHCs in the basal turn. (b) A DTR mouse cochlea without DT injection also shows a single row of IHCs and three rows of OHCs in the basal turn as well. (c and d) A DTR mouse cochlea with DT injection at P25 demonstrates no IHCs or OHCs in the basal turn (c) and the apical turn (d). OHC: outer hair cells; IHC: inner hair cells; PC: Pillar cells, DC: Deiters cells, and ISC: inner supporting cells. **B):** Immunohistochemistry of transplanted hESC-derived ONP spheroids in the DTR mouse cochlea. Left column: a corresponding low-power magnification microphotograph of the DTR mouse cochlea (10X). Each yellow circle indicates the anatomical location of a transplanted hESC-derived ONP spheroid. Right column: high-power magnification microphotographs of transplanted hESC-derived ONP spheroids stained with TOTO3 (nuclear counterstaining), β-III tubulin, and AHNA (40X). (a) Human ESC-derived ONP spheroids transplanted with 1% GrowDex®-T. (b) Human ESC-derived ONP spheroids transplanted with 1% GrowDex®-T and 800,000 of PODS®-hBDNF. Small white arrow: neurites. (c) Another hESC-derived ONP spheroid transplanted with 1% GrowDex®-T and 800,000 of PODS®-hBDNF. SM: scala media, SV: scala vestibuli, ST: scala tympani, MT: the middle turn of the cochlea, and MO: modiolus. **(C):** (a) Quantification of the number of ANHA positive cells (profile) in three different turns of the DTR mouse cochleae. (b) Quantification of the number of the ANHA positive cells (profile) in dissociated ONPs transplantation vs. ONP spheroids transplantation in four anatomical subdivisions of the cochlea. (c) Quantification of the number of the triple positive cells (profile) in dissociated ONPs transplantation vs. ONP spheroid transplantation with three

different substrates. (d): Quantification of the number of neurites in dissociated ONPs transplantation vs. ONP spheroid transplantation. NIM: neuronal induction media, G: GrowDex®-T, G+P: GrowDex®-T and PODS®-hBDNF. *$p < 0.05$, ** $p < 0.01$, N.S.: not significant by one-way ANOVA with Tukey's *post-hoc* test. Note that all of the images stained for TOTO3 iodide and AHNA have been pseudo-colored. **(D):** Calcofluor White staining indicates the presence of NFC at both seven days and ninety days post-transplantation. **(E):** Tissue response in H&E histology. (a) Control WT cochlea (no surgery). (b) DTR mouse cochlea transplanted with hESC-derived ONP spheroids with GrowDex®-T and PODS®-hBDNF. The DTR mouse was euthanized seven days after the transplant surgery (D10). (c) DTR mouse cochlea transplanted with hESC-derived ONP spheroids with GrowDex®-T and PODS®-hBDNF. The DTR mouse was euthanized 90 days after the transplant surgery (D90). **(F):** Expression of MHC class I and MHC class II proteins assessed by flow cytometry in undifferentiated hESCs (H9) and hESC-derived ONP spheroids (ONPs). Red lines represent background staining with the conjugated antibody (MHC I and MHC II) alone. Three independent experiments were performed and the results were averaged for each analysis.